ESD-TR-71-191

Semiannual Technical Summary

Seismic Discrimination

30 June 1971

Prepared for the Advanced Research Projects Agency
under Electronic Systems Division Contract F19628-70-C-0230 by

Lincoln Laboratory

MASSACHUSETTS INSTITUTE OF TECHNOLOGY

Lexington, Massachusetts

DOCUMENT CONTROL DATA - R&D

(Security classification of title, body of abstract and indexing annotation must be entered when the overall report is classified)

1. ORIGINATING ACTIVITY *(Corporate author)*
Lincoln Laboratory, M.I.T.

2a. REPORT SECURITY CLASSIFICATION
Unclassified

2b. GROUP
None

3. REPORT TITLE
Seismic Discrimination

4. DESCRIPTIVE NOTES *(Type of report and inclusive dates)*
Semiannual Technical Summary Report - 1 January through 30 June 1971

5. AUTHOR(S) *(Last name, first name, initial)*
Davies, David

6. REPORT DATE
30 June 1971

7a. TOTAL NO. OF PAGES
68

7b. NO. OF REFS
39

8a. CONTRACT OR GRANT NO. F19628-70-C-0230
AF 49(638)-1763

b. PROJECT NO. ARPA Order 512

c.

d.

9a. ORIGINATOR'S REPORT NUMBER(S)
Semiannual Technical Summary
30 June 1971

9b. OTHER REPORT NO(S) *(Any other numbers that may be assigned this report)*
ESD-TR-71-191

10. AVAILABILITY/LIMITATION NOTICES
Approved for public release; distribution unlimited.

11. SUPPLEMENTARY NOTES
None

Details of illustrations in this document may be better studied on microfiche

12. SPONSORING MILITARY ACTIVITY
Advanced Research Projects Agency, Department of Defense

13. ABSTRACT

Progress in the definition of spectral characteristics of explosions and earthquakes and in the determination of their time functions is reported. The complexities of surface wave and body wave propagation in a heterogeneous Earth are further considered, and the coherence of seismic signals is discussed with reference to different mantle regions. A technique for computing signals reflected from transition layers is given. The first NORSAR data show travel-time anomalies much more complex than could be associated with sub-NORSAR structure. NORSAR spectraforms are described for several Asian events. A transfer function technique is used to determine sub-LASA structure. Significance tests for Vespagram and Beamsplit displays are described. Upgrading of the Lincoln data analysis facilities is reported.

14. KEY WORDS
seismic array seismometers seismology

BLANK PAGE

MASSACHUSETTS INSTITUTE OF TECHNOLOGY

LINCOLN LABORATORY

SEISMIC DISCRIMINATION

SEMIANNUAL TECHNICAL SUMMARY REPORT
TO THE
ADVANCED RESEARCH PROJECTS AGENCY

1 JANUARY – 30 JUNE 1971

ISSUED 2 AUGUST 1971

LEXINGTON MASSACHUSETTS

The work reported in this document was performed at Lincoln Laboratory, a center for research operated by Massachusetts Institute of Technology. This research is a part of Project Vela Uniform, which is sponsored by the Advanced Research Projects Agency of the Department of Defense under Air Force Contract F19628-70-C-0230 (ARPA Order 512). Part of the work reported herein is supported by Air Force Contract AF 49(638)-1763 with Massachusetts Institute of Technology.

ABSTRACT

Progress in the definition of spectral characteristics of explosions and earthquakes and in the determination of their time functions is reported. The complexities of surface wave and body wave propagation in a heterogeneous Earth are further considered, and the coherence of seismic signals is discussed with reference to different mantle regions. A technique for computing signals reflected from transition layers is given. The first NORSAR data show travel-time anomalies much more complex than could be associated with sub-NORSAR structure. NORSAR spectraforms are described for several Asian events. A transfer function technique is used to determine sub-LASA structure. Significance tests for Vespagram and Beamsplit displays are described. Upgrading of the Lincoln data analysis facilities is reported.

Accepted for the Air Force
Joseph R. Waterman, Lt. Col., USAF
Chief, Lincoln Laboratory Project Office

CONTENTS

SUMMARY

This is the fifteenth Semiannual Technical Summary of the Seismic Discrimination Group of Lincoln Laboratory. The aim of this work is to extend our understanding of the theoretical background and observational results concerned with the detection and identification of underground nuclear explosions, in order to provide such technical information as may be required in discussions of an underground nuclear test ban. Our work is mainly, but by no means exclusively, tied to the effective use of large arrays. Up to the present we have predominantly considered LASA in our publications; however, with the recent completion of ALPA and NORSAR we anticipate intensive study of these two arrays in the coming year.

Since the general acceptance of the M_s:m_b technique as a means of discriminating between earthquakes and explosions, the seismological community has devoted considerable time to answering the following questions:

(a) Can the threshold at which this discriminant works be lowered by improved global instrumentation?

(b) Is there a sound scientific basis for discrimination and does this predict a size of event below which conventional seismic techniques will see no distinctions?

(c) Can the determinations of M_s and m_b be made more reliable, particularly at low magnitudes, or at least can the reason for the frequent large scatter in values be well understood?

(d) Are there any further discriminants which might work to a lower threshold or supplant M_s:m_b in certain cases?

To help to answer these questions our work continues on a broad base which we divide in this report into four sections: Seismic Source Characteristics, Propagation Path, Receiver and Data Processing Schemes, and Lincoln-Based Data Processing Facilities.

We have used LASA in extending previous studies of the spectral characteristics of earthquakes and explosions in the Western U.S. The total spectrum (both short and long period) is now available for analysis. It is also possible to calculate the integrated spectrum in these two bands. Comparisons are made between the Rayleigh-wave energy and the P-wave energy for explosions and earthquakes in order to see to what degree the energy is partitioned. Preliminary results show that there is separation, although not by an entirely satisfactory amount without some restrictions on window lengths and spectral bands.

The strange nature of inner core reflections of NTS explosions is considered further with an attempt to fit a source time function of an explosion to the pulse shape. We conclude that the ground displacement in the vicinity of the source has a very strong impulsive component, and that the "width" of the impulse is about 2 sec for a 1 Mt explosion. If the near source displacement behavior of all explosions is dominantly an impulse, the basis for discrimination would lie in the spectral differences between impulses and steps – more characteristic of earthquakes.

A suite of earthquakes in the Kuriles region reveals a striking distinction between two practically parallel and widely separated sets of events using the M_s:m_b technique. Neither population overlaps with any possible explosion line, but we have a unique opportunity to attempt to find what differs between the two earthquake types. It is concluded that the dimensions of the earthquakes control the separation through the duration of the event and consequent spectral effects.

Summary

A study of explosion BOXCAR as recorded at NORSAR has been made in order to fit the P-wave shape to theoretical explosion and propagation characteristics. A high degree of similarity can be obtained using a Haskell model of the explosive source and a value for t* (the attenuation parameter) of 0.5.

Attempts to explain the nature of the P-wave amplitude variation associated with explosion Longshot have now proved successful. The three-dimensional ray tracing program and the observations of high and low amplitude signals in various regions assumed to be due to focussing and defocussing have been brought together, in conjunction with a geophysically reasonable model of the Aleutian arc, to yield good agreement. The influence of upper-mantle structure on the estimate of m_b is profound.

The multipath studies of Rayleigh waves reported in recent SATS have been extended to Love waves and it is demonstrated that the same general sources of multipathing occur in both cases, namely internal reflections from continental margins. Striking similarity is reported between Love and Rayleigh multipathing for some events, but there are some for which the two wave types seem to undergo different reflections.

Short period seismic waves from presumed explosions in different regions of the Soviet Union have remarkably different codas. We show events from two regions in which the coherency of the coda is very different. A coherent coda can be explained in terms of near source structure, such as horizontal layering; while an incoherent coda, it seems, must be ascribed to some sort of scattering process. This process cannot be under LASA, so we conclude that it must take place in the mantle beneath the Soviet Union. It is important for two reasons – one is that magnitude estimates should take account of energy content within the coda and the other is that we may have in coherency a very interesting geophysical observation on the microstructure of the Upper Mantle.

Determination of the nature of the signal reflected and transmitted at a boundary for which properties vary over a distance comparable to a wavelength has importance in any attempt to use P-wave signals to understand source characteristics. New time-domain solutions are reported for simple models in which both velocity and density may vary smoothly through the boundary.

On the basis of the first data to be received from NORSAR we have been able to estimate the travel time anomalies associated with that array. The most notable thing to emerge so far has been the strong correlation of the azimuthal error (arising from fitting a plane wave to the incoming signal) with the tectonic region.

Further results of spectraforming are presented. NORSAR (which is particularly suitable for this process) reveals a number of events in Iran which have particularly strong high frequency content. These events are considered in detail.

A discussion is given of the significance levels that may be associated with Vespagram and Beamsplit displays. Definitions of a seismic "signal" and "noise" are given within the context of the complicated output that these programs present to an analyst. An example of a P-wave signal undergoing a complicated reflection at a sloping continental shelf is used to illustrate the significance levels.

The crustal transfer function ratio of Phinney has been used in an effort to extract crustal parameters from LASA data. Vertical and horizontal long period instruments at many sub-arrays

were used and a clear trend was found for the period of the function's peak, indicating a general thinning of the crust in a westerly direction.

Peculiar very long period signals from LASA have been reported in the past, and there has been some question of their reality. Further analysis has revealed the strong possibility that these signals arise from intermodulation distortion when a short period Rg phase travels across the array.

Continued improvements in our data analysis facilities are reported. A high grade printer-plotter is now available to either PDP-7 computer for hard-copy output.

The Lincoln daily bulletin continues to be produced from visual observation of LASA data. Its capabilities were described in the last SATS. It is available on a routine basis to those who may need quick information about seismic events.

D. Davies

GLOSSARY

ALPA	Alaskan Long Period Array
LASA	Large Aperture Seismic Array, Billings, Montana
NORSAR	Norwegian Seismic Array
NTS	Nevada Test Site
PDE	Preliminary Determination of Epicenter
SATS	Semiannual Technical Summary
TFSO	Tonto Forest Seismological Observatory
USCGS	United States Coast and Geodetic Survey
VESPA	Velocity Spectral Analysis

SEISMIC DISCRIMINATION

I. SEISMIC SOURCE CHARACTERISTICS

A. SPECTRAL STUDIES OF EXPLOSIONS AND EARTHQUAKES

In previous SATS reports we have discussed in detail certain aspects of the seismic spectrum of underground explosions as separately recorded in long and short period response bands. We have now begun a study in which we combine both the short and long period spectral data from explosions and earthquakes in order to understand better the generic differences of the two source types and to discriminate between them. The work reported shows progress in this endeavor.

At this stage of the study we have considered only Nevada Test Site (NTS) explosions and a few earthquakes from the southwestern United States as recorded at LASA. Because of the complicated nature of the P-wave arrival at these distances and the content of the Lincoln data library, the inferences concerning the nature of the short period spectrum must be somewhat qualified. Typically, for example, the recorded short period P-wave motion at LASA from NTS events has a duration of 1.5 to 3.0 min. depending upon the size of the explosion. We have arbitrarily taken the first 100 sec of this motion as representative of the short period radiated from these regional sources. We do this because it is most difficult to differentiate between the various crustal and upper mantle phases using these records. Despite the uncertainty in the nature of the path, we have used this motion to measure the relative short period excitation of events at about the same distance from LASA. Additionally, most of the short period data in the Lincoln library is that of undelayed subarray sums which are not practical for low velocity, regional P-waves. Some single sensor data are available for the explosions and we have used these data to get a more complete look at the explosion spectrum. However, when comparing earthquake with explosion spectra we are forced to use the subarray sum data for both. At long periods we have used the vertical component of the Rayleigh wave, as discussed in the last SATS (31 December 1970, DDC AD-718971), except for a reduced window length to eliminate a late arriving long period motion at some sensors which may be spurious (see Sec. III).

The nature of the short period data used is shown in Fig. I-1 where the recorded motion at the center seismometer of the D1 subarray from the NTS event Jorum and the computed spectrum are displayed. There is considerable detail shown by the computed spectrum, so that the diagrams that follow the short period data are smoothed and corrected for instrument response, and absolute scaling is maintained. No attempt has been made to correct the spectra for the effects of propagation; however, most of the events considered are at about the same distance and azimuth from LASA.

Figure I-2 shows the P- and Rayleigh-wave spectra from the three NTS explosions at Pahute Mesa. The events used, the USCGS body wave magnitudes assigned (m_b), and the yield estimates by Springer and Kinnamann[1] are listed.

Event	USCGS (m_b)	Approximate Yield
Jorum	6.2	1 Mt
Purse	5.8	20 to 200 kt
Pipkin	5.5	200 to 1000 kt

Figure I-2 shows the essential features of the far-field seismic spectrum from explosions. The first of these is that as yield increases the relative increase in spectral amplitudes at long periods is much greater than that at short periods. In other words, at 20 sec, the spectral amplitude of Jorum is at least an order of magnitude larger than the two smaller explosions, while at 1 sec, Jorum is less than half an order of magnitude larger. This phenomenon is predicted by various simple analytical models for the explosive source. Secondly, even though from this single station measurement Purse is apparently slightly larger than Pipkin, the long period spectra are much more well ordered than the short period spectra. The long period spectra rarely cross and appear to increase monotonically with frequency over most of the relevant long period band, whereas the short period spectra are more complicated. Last, the long period spectra of larger explosions show higher spectral amplitudes at 30 sec relative to 10 sec. This can be interpreted as an increase in the decay time of the pressure pulse of the larger explosions. These conclusions are based on a number of events greater than those depicted in Fig. I-2, which shows only the three for clarity.

Figure I-3 shows the short and long period spectra for the three Yucca Flat events:

Event	USCGS (m_b)	Yield Estimates[1] (kt)
Grape-A	5.5	20 to 200
Hutch	5.6	200 to 1000
Terrine	5.2	20 to 200

In this case, the picture is slightly less clear in that the long period spectrum of Hutch shows contamination by a small interfering event from the Aleutians and, according to Springer and Kinnamann,[1] the source medium of Hutch is alluvium as opposed to tuff for Grape-A and Terrine. In general, however, the long period spectra of Fig. I-3 show less complication than the short period spectra and it can be seen that at these lower magnitudes the separation of the spectra at 20 sec and at 1 sec is roughly the same.

Recently we have begun to apply this method of total spectral comparison to earthquakes and at present we can report the results of the comparison using only three earthquakes. They are:

	4 October 1967	28 September 1967	28 April 1969
Origin Time (GMT)	10:20:14.0	15:38:35.9	23:20:42.9
Latitude (°N)	38.5	37.2	33.4
Longitude (°W)	112.1	121.6	116.4
Depth (km)	18 ± 6	2	20
m_b	5.2	5.5	5.2
Δ (deg)	9.3	14.8	15.4
Azimuth (deg)	210.0	235.8	212.5

These parameters are those assigned by the USCGS. These earthquake spectra are plotted in Fig. I-4 where they can be compared with the spectrum of the explosion Purse. The short period spectra in this case are all computed from subarray sum traces. It is seen in Fig. I-4 that the earthquake long period spectra show a greater variability than the explosions, although the short period spectra are of generally the same shape. Perhaps a more direct comparison can be made from Fig. I-5 where we have normalized all the events of Fig. I-4 at 20 sec period. When normalized at 20 sec, all the earthquakes of Fig. I-5 exhibit less spectral content at 1 sec than the explosion Purse. However the difference at 1 sec between two of the earthquakes and the explosion is not overwhelming (about half an order of magnitude). Recently Molnar, et al.,[2] have suggested a long period spectral discriminate using the ratio of surface wave amplitudes at 20 sec to those in the period range 40 to 60 sec. According to Fig. I-5, two of the three earthquakes would not separate from the explosion using such a criterion here. Although these data are obtained from narrow band, long period instruments, we feel the size of these events is such that Fig. I-5 gives a fairly accurate picture of the relative amplitudes of the long period ground motion at LASA.

Figure I-6 represents a preliminary attempt to discriminate between explosions and earthquakes using the total energy in long and short period spectral bands. The ordinate in Fig. I-6 is proportional to spectral energy of the vertical component of the Rayleigh wave, (SE_R), the abscissa is proportional to spectral energy in the P-wave (SE_p). Here

$$SE_p = \Sigma A_p^2 f^2 \qquad 3.0 \geq f \geq 1.0 \text{ cps}$$

$$SE_R = \Sigma A_R^2 f^2 \qquad 0.02 \leq f \leq 0.1 \text{ cps},$$

where A is spectral amplitude as shown in previous figures and f is frequency in cps. Points plotted as circles are those where single sensors were used to compute the short period spectra. Subarray sums were used for the points plotted as triangles. Both types of data were used for the explosions Purse and Pipkin and the deterioration of the spectrum due to summing can be seen in a shift to the left in the short period energy. There is some separation indicated in Fig. I-6, yet the results cannot be considered completely encouraging. However, at this stage we have not attempted to optimize the separation by varying time window lengths and spectral energy bands.

J. Filson
L. Lande

B. SOURCE-TIME FUNCTIONS FOR EXPLOSIONS

One surprisingly unsolved problem in seismic discrimination is that of the nature of the source-time function for an explosion. By source-time function I mean the temporal variation of displacement of any particular point in the vicinity of the explosion. The matter is very important, for if it could be established that the spectra of explosions and small volume earthquakes were fundamentally different across the $4\frac{1}{2}$ octave span from 1 to 20 sec periods, the basis for discrimination would evidently be primarily in the source-time function rather than in the extent of the event, its depth or mechanism, which are other suggested candidates.

TABLE I-1

M_s-m_b DATA FOR A SUITE OF KURILE-KAMCHATKA EARTHQUAKES
(Group A – M_s high relative to m_b; Group B – M_s low relative to m_b)

Group	Date	Time	Latitude (°N)	Longitude (°E)	Depth (h) (km)	m_b (USGS)	m_b (LASA)	Complexity (LASA)	M_s (LASA)
A	3/25/67	22:47:58	45.45	151.41	41	5.5	5.64	8.9	5.35
	4/1/67	12:23:36	54.70	151.79	40	5.9	5.90	5.7	5.57
	4/1/67	14:00:34	45.84	151.74	23	5.4	5.63	6.0	4.81
	12/16/67	20:53:58	51.22	157.66	24	5.5	5.87	5.7	5.63
	1/24/68	14:29:43	54.67	167.92	N	4.3	4.38	7.0	3.64
	1/29/68	10:19:06	43.62	146.66	40	6.3	6.29	7.2	6.5
	1/29/68	16:42:50	43.49	147.20	36R	5.7	5.95	7.2	5.65
	1/29/68	17:14:06	43.36	147.29	N	4.5	4.72	7.6	4.19
	1/30/68	01:30:13	43.27	146.79	12	5.3	5.02	3.6	4.53
	1/30/68	01:48:29	43.25	147.68	N	5.1	5.28	9.6	4.97
B	11/21/66	12:19:27	46.68	152.46	40R	5.6	6.20	1.4	4.58
	12/7/66	17:17:42	44.26	151.67	26	5.8	6.24	3.1	4.76
	6/7/67	18:16:31	47.45	155.44	29	5.2	5.64	1.5	4.08
	10/5/67	15:55:03	45.43	150.72	N	5.3	5.62	1.3	4.32
	10/7/67	08:28:01	49.20	156.27	N	5.3	5.75	5.0	4.45
	11/1/67	16:30:57	48.27	154.36	40	5.5	5.81	2.5	4.20
	12/14/67	18:25:17	54.57	160.43	N	5.5	5.41	2.2	4.02
	12/23/67	16:04:38	48.25	157.28	26	5.1	5.70	1.6	3.21
	1/2/68	07:30:12	45.67	150.92	87	4.7	4.99	2.1	3.77
	1/3/68	07:49:04	54.87	161.49	39	4.8	5.01	1.1	3.40
	1/11/68	18:08:38	46.43	153.29	50	4.7	5.02	7.6	3.76

Recently Wyss, et al.,[3] and Molnar[4] have examined long-period instrument recordings of large explosions. These records are visibly very different from characteristic earthquake records and consist, typically, of one cycle of signal with a period of 3 or 4 sec. It seems inescapable that this indicates a source function more complicated than a simple step function – probably containing an impulsive component.

In the last SATS (31 December 1970, DDC AD-718971) I described observations of PKiKP which showed a strange double pulse for large explosions in Nevada recorded at LASA.

More reeent work has made it more likely than ever that this is a source effect. Figure I-7 shows the striking similarity of PKiKP and PcP for Nevada explosions. This rules out any lingering doubts that the effect might have been one of the propagation path. Figure I-8 is an attempt to model the observed Boxcar PKiKP signal as two Haskell analytic source functions[5] of opposite polarity convolved with the Earth's attenuation response and the instrumental response. The fit is sufficiently good for it to be asserted that the model of near source displacement in Fig. I-8 is in broad detail that of Boxcar; that is, a broad impulse with sharp beginning and end, leading to a pair of short impulses in the far field. The final displacement level is open to discussion, but it seems that the broad impulse must dominate the source-time function. Elastodynamic theory for a step function in pressure is inadequate to describe this overshoot so we must conclude that the explosion itself puts a broad impulse on the walls of the equivalent cavity.

If the above discussion is correct and our conventional understanding of earthquakes as representing steps in displacement near source is also valid, then the spectral content of explosions and earthquakes at source is fundamentally different and a factor-of-20 difference in Rayleigh wave excitation at 20 sec would be expected when two events had the same body wave magnitude at 1 sec. This distinction is not grossly out of line with observations made using the M_s:m_b discriminant. The distinetion is also relatively magnitude independent.

D. Davies

C. MAGNITUDES AND SOURCE CHARACTER

Table I-1 gives data for an interesting suite of earthquakes in the Kurile-Kamchatka region. The USCGS data were obtained from PDE reports and the LASA parameters obtained as described in detail in an earlier report.[6] Briefly, the LASA M_s is obtained by chirp filtering of a long period vertical beam, complexity is computed from the best LASA short period beam, and m_b is calculated from the largest excursion of the short period beam, with no restriction to the first few cycles after onset. Figure I-9 is a M_s-m_b plot of the LASA data and shows clearly that there are two distinct populations, corresponding to groups A and B of Table I-1.

One might be tempted to assert that the separation in Fig. I-9 is due primarily to the peculiar way in which m_b was measured at LASA and the use of a single station for m_b measurements, rather than a network. However the peak short period excursion for all events in class B was in the first few cycles; but, with one exception, in class A the peak on the LASA beam was several seconds into the waveform. So if the LASA m_b were calculated using traditional methods the two classes would be even more distinct. Also, if the USCGS m_b is used rather than the LASA m_b the populations still retain their identities although they are slightly closer together. We have not yet experimentally determined the impact of using a network M_s value rather than the LASA

value. Even without doing that we can say there are two distinct kinds of earthquakes in our population. The differences may be in fault type or orientation, stress release levels, rupture dimensions, etc., and are not normalized out in obtaining magnitudes. Said differently, m_b from a network or single station is at best a very crude measure of radiated short period P-wave energy. M_s may be somewhat better for surface wave energy in the 20 sec band, but it also leaves a great deal to be desired.

Davies pointed out in a recent SATS (30 June 1970, DDC AD-710613) the large effect which lateral inhomogeneities in the upper mantle can have upon the waveform complexity and magnitude measured at a single station. More on this point is included in Sec. II of this report. It appears that the effect of a downthrusting plate can be large but should be confined to stations located in a relatively limited angle behind the plate. LASA does not lie in that area with respect to the plate in the Kurile Island region. For this reason we do not believe the plate can significantly distort initial short period arrivals from this region as recorded at LASA. Also, the two populations do not clearly separate on the basis of USCGS location, although there are five events clustered at the southern end of the chain which all have large M_s values.

It is reasonable to believe that events with large short period time durations might generate considerably larger surface waves than small time duration events from the same region. This definitely seems to be the case for the events in Table I-1. Event complexity, roughly the ratio of integrated signal amplitude change in the first five seconds to the integrated amplitude for the next thirty seconds, is high for the events with high surface wave magnitudes. This high complexity is probably a result of the source time duration rather than a path effect. If the m_b value for events with high complexity were increased in some way to account for that fact then the scatter in the $M_s - m_b$ plot might be reduced. This possibility and others directed toward obtaining a more stable measure of short period P-wave energy are now being investigated.

R. T. Lacoss

D. PREDICTION OF TELESEISMIC P-WAVE SHAPES FROM EXPLOSIONS

Attempts are being made to predict the shape of teleseismic P-waves from explosions. This has been done by Carpenter,[7] for example, assuming impulsive source models with rise times much faster than the peak instrument response.

We consider a particular source model given by Haskell[5] and calculate the P-waves recorded by the NORSAR digital system. The shape of the signal is assumed to be controlled by four factors: source function, source depth, average attenuation through the Earth, and the recording system. Layering and scattering effects of the Earth along the transmission path are not considered, nor is spherical spreading included.

At teleseismic distances, the effective shape of the ground displacement source, $u(\tau)$, is given by the derivative of the reduced displacement potential, $\psi(\tau)$. Assuming Haskell's analytic approximation for $\psi(\tau)$, based on near-in explosion data, the source function is

$$u(\tau) = K\psi(\infty)\, e^{-K\tau} [(4B + 1/6) - BK\tau] (K\tau)^3 \qquad \text{(I-1)}$$

where B is a function of the medium only and $\psi(\infty)$ is proportional to the yield Y in kilotons. For a given explosion medium, the parameter K controls the time scale of the source function.

K^{-1} scales with yield and depth in the same way that the equivalent elastic radius scales for contained explosions. Using Mueller's expression[8] for scaling elastic radii, we obtain

$$\frac{K}{K_o} = \left(\frac{Y}{Y_o}\right)^{-1/3} \left(\frac{h}{h_o}\right)^{1/2.4} \qquad \text{(I-2)}$$

where K_o, Y_o and h_o are values of Haskell's parameter K, of the yield and of the burial depth, respectively, for a reference explosion in the same medium as the explosion to be estimated.

As an example we consider the NTS event Boxcar,[1] of yield Y ~ 1200 kt, detonated on 26 April 1968, at depth h = 1.16 km in rhyolite, which is a finely grained granite. The event Hardhat[9] was chosen as the reference event. It was detonated on 15 February 1962 with a yield Y_o ~ 5 kt, at depth h_o = 0.287 km in granite. For this event, Haskell assigned a value of $K_o = 31.6\ \text{sec}^{-1}$. Substituting the above values into Eq. (1-2) we obtain $K = 9.2\ \text{sec}^{-1}$. Putting this K and Haskell's value of B = 0.24 for granite into Eq. (1-1), we obtain the simulated source function for Boxcar shown at the top of Fig. 1-10.

The effect of the Earth's attenuation over the short period band is approximated by a constant Q operator, which to be realistic, must have a phase shift associated with the exponential attenuation. Carpenter's form[7] of the attenuation operator has the Fourier transform

$$a(\omega) = \exp\left[-\frac{\omega t^*}{2} + i\omega\,\frac{t^*}{\pi}\left\{\ln\left(\frac{\omega}{\omega'}\right) - 2\right\}\right] \qquad \text{(I-3)}$$

for $0 \leqslant \omega \leqslant \omega'$. The parameter $t^* = T/Q_{AV}$, T being the travel time of the P-wave, and Q_{AV} the average quality factor over the propagation path. ω' is the highest frequency used in the Fourier synthesis of the time domain operator $A(\tau)$. For a digital operator sampled every 0.05 sec, ω' is taken to be 20π rad/sec, the foldover frequency.

The short period seismometers at NORSAR are similar in response to those at LASA. They have a natural frequency f_n = 1 cps and a damping factor d = 0.707. Before digitization of the signal, a four pole Chebyshev filter is applied to the analog data to cut off frequencies above 5 cps.

The time domain synthesis of the combined attenuation and instrument responses are shown in the middle row of traces of Fig. 1-10 for several values of assumed t*. The convolution of the source function with each of these operators is shown in the bottom row of traces in the same figure.

Superposed on the synthetic P-wave for t* = 0.5 is the digital recording of Boxcar at the Oyer subarray of NORSAR. The width of the actual P-wave suggests that a t* slightly less than 0.5 in the theoretical response adequately explains the data. Filson (SATS, 31 December 1970, DDC AD-718971) measured t* for the NTS to Oyer P-wave path by computing the spectral ratio of near-in displacement meter recordings of Boxcar to the P-wave at Oyer. The average of his values of t* is 0.36. In view of the uncertainties in seismic scaling from low to high yields, these two estimates of t* agree reasonably well. The surface reflection at NTS, i.e., pP, is apparently not required to fit the observed data at Oyer. This suggests that the free surface reflection coefficient must be considerably less than 1 in magnitude and cannot be approximated by plane wave or ray theory.

C. W. Frasier

REFERENCES

1. D. L. Springer and R. L. Kinnamann, "Seismic Source Summary for U.S. Underground Nuclear Explosions 1961-1970," UCRL-73036 Preprint, Lawrence Radiation Laboratory, University of California (26 February 1971).
2. P. Molnar, J. Savino, L. R. Sykes, R. C. Liebermann and G. Hade, "Small Earthquakes and Explosions in Western North America Recorded by New High Gain, Long Period Seismographs," Nature 224, 1268-1273 (1969).
3. M. Wyss, T. C. Hanks and R. C. Liebermann, "Comparison of P-Wave Spectra of Underground Explosions and Earthquakes," J. Geophysics Res. 76, 2716 (1971).
4. P. Molnar, "P-Wave Spectra from Underground Nuclear Explosions," Geophys. J. (in press).
5. N. A. Haskell, "Analytic Approximation for the Elastic Radiation from a Contained Underground Explosion," J. Geophys. Res. 72, 2583 (1967).
6. R. T. Lacoss, "A Large Population LASA Discrimination Experiment," Technical Note 1969-24, Lincoln Laboratory, M.I.T. (8 April 1969), DDC AD-687478.
7. E. W. Carpenter, "Teleseismic Signals Calculated for Underground, Underwater, and Atmospheric Explosions," Geophysics 32, 17-32 (1967).
8. R. A. Mueller and J. R. Murphy, "Seismic Characteristics of Underground Nuclear Detonations, Part I" (submitted to Bull. Seismol. Soc. Am.).
9. G. C. Werth and R. F. Herbst, "Comparison of Amplitudes of Seismic Waves from Nuclear Explosions in Four Mediums," J. Geophys. Res. 68, 1463-1475 (1963).

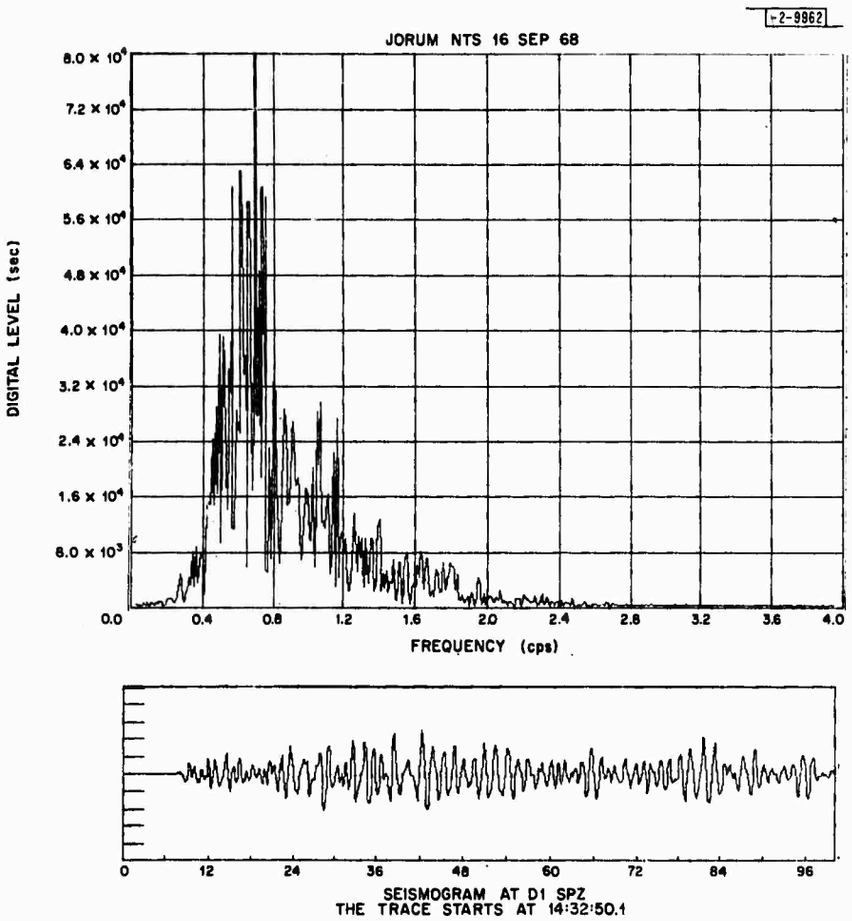

Fig. I-1. Short period seismic trace from the center seismometer of subarray D1 and the associated spectrum. The motion is due to the NTS event Jorum.

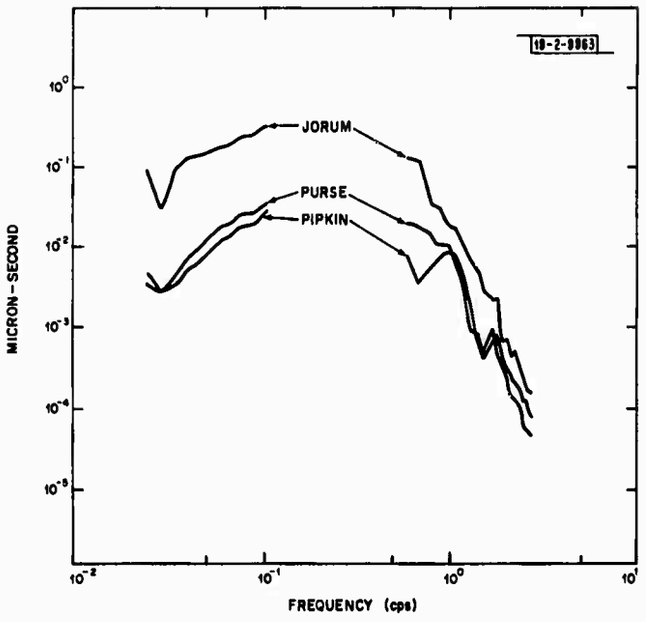

Fig. I-2. Scaled Rayleigh and P-wave spectra from three Pahute Mesa explosions recorded by single sensors at subarray D1.

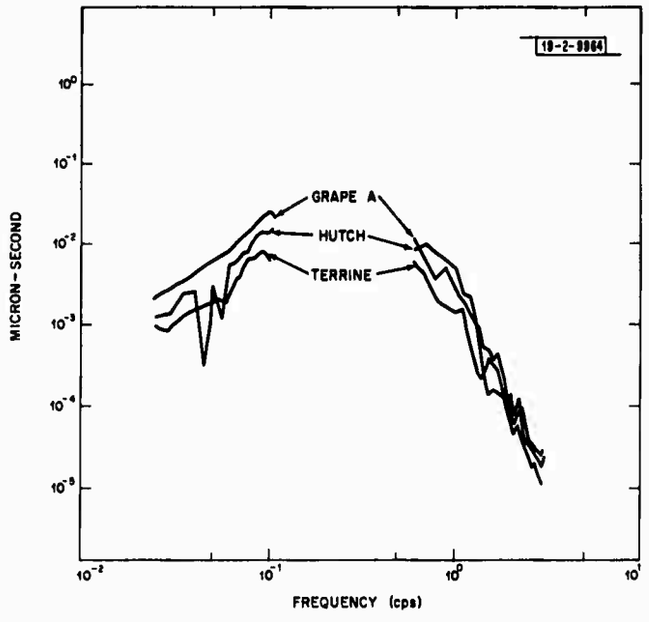

Fig. I-3. Scaled Rayleigh and P-wave spectra from three Yucca Flat explosions recorded by single sensors at subarray D1.

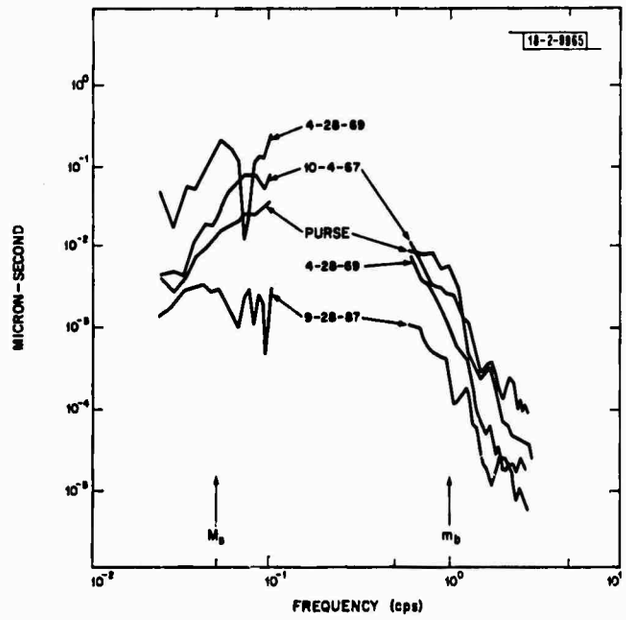

Fig. I-4. Scaled Rayleigh and P-wave spectra from the NTS event Purse and three earthquakes. In this case the D1 subarray sum was used to compute the short period spectra.

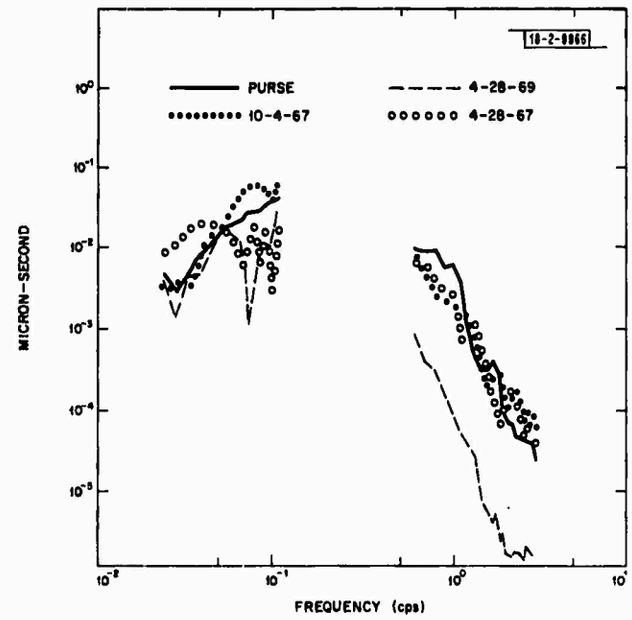

Fig. I-5. Same data as Fig. I-4 with all spectra normalized at 20 sec period.

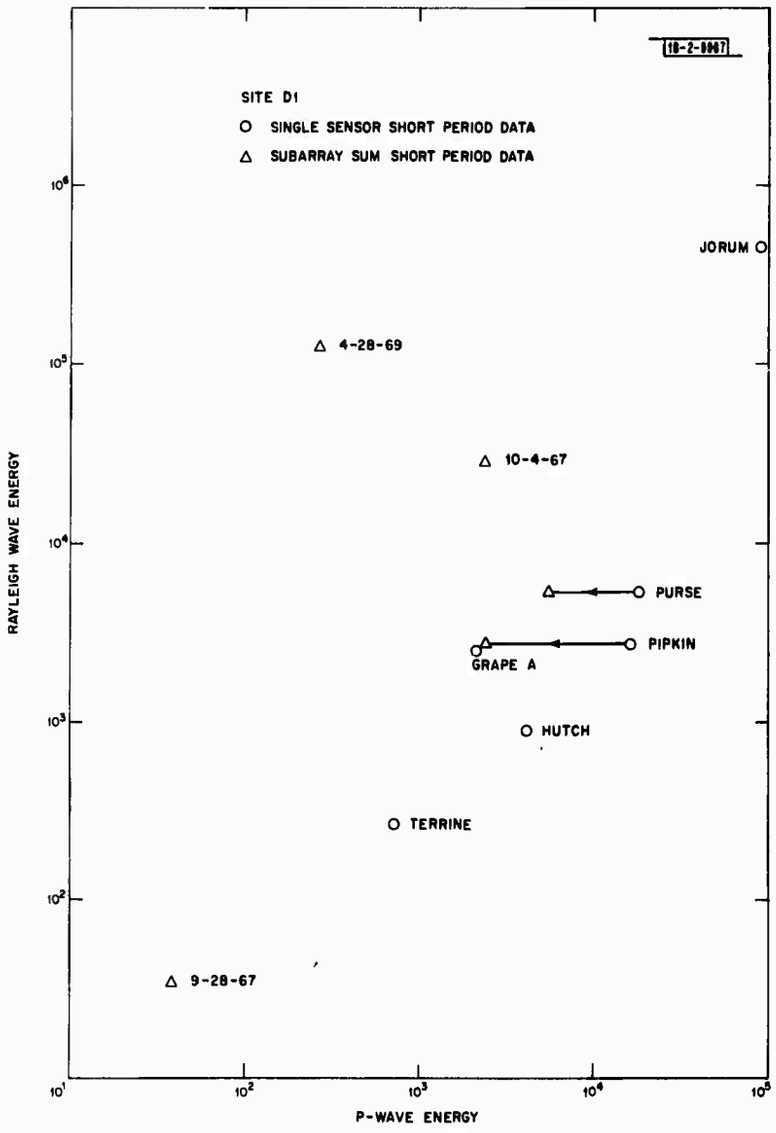

Fig. I-6. Relative spectral energies in Rayleigh and P-waves of events used in this study.

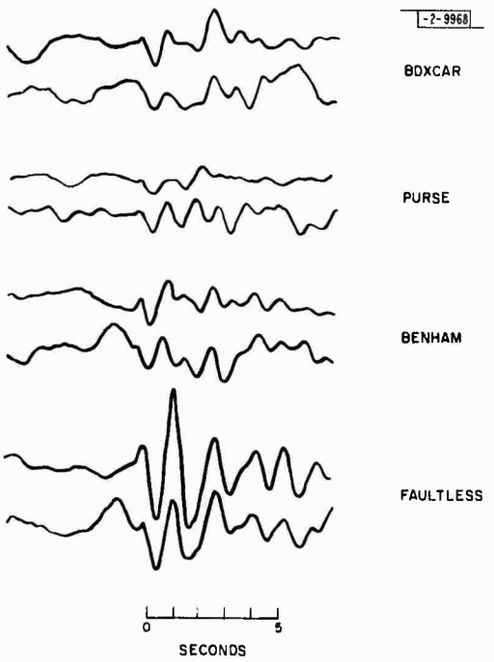

Fig. I-7. PKiKP (upper) and PcP (lower) signals from large undergraund explosians in Nevada.

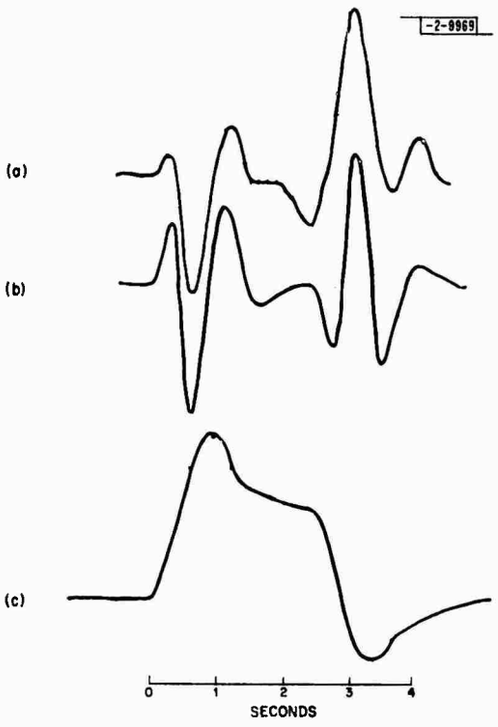

Fig. I-8. (a) PKiKP from Boxcar, (b) a fit ta this signal and (c) the near saurce displacement necessary ta produce signal (b).

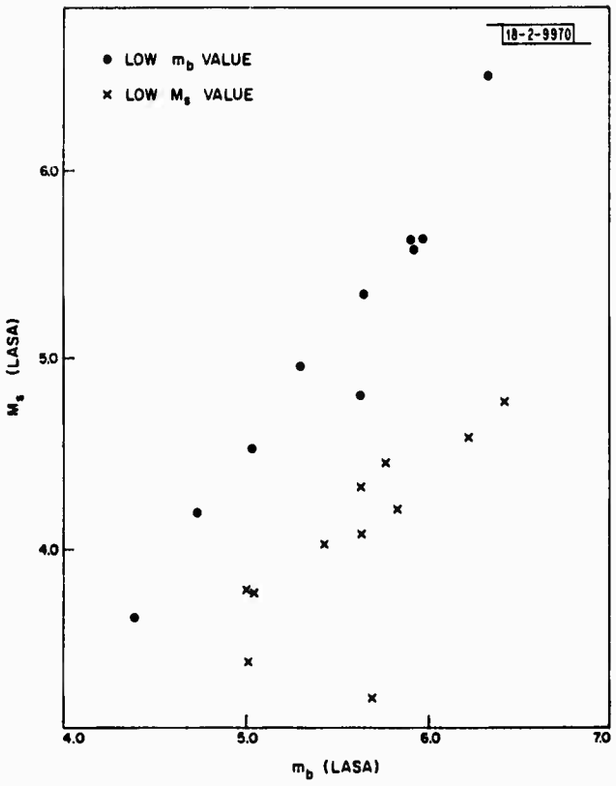

Fig. I-9. LASA M_s:m_b plot for Kurile Island earthquakes.

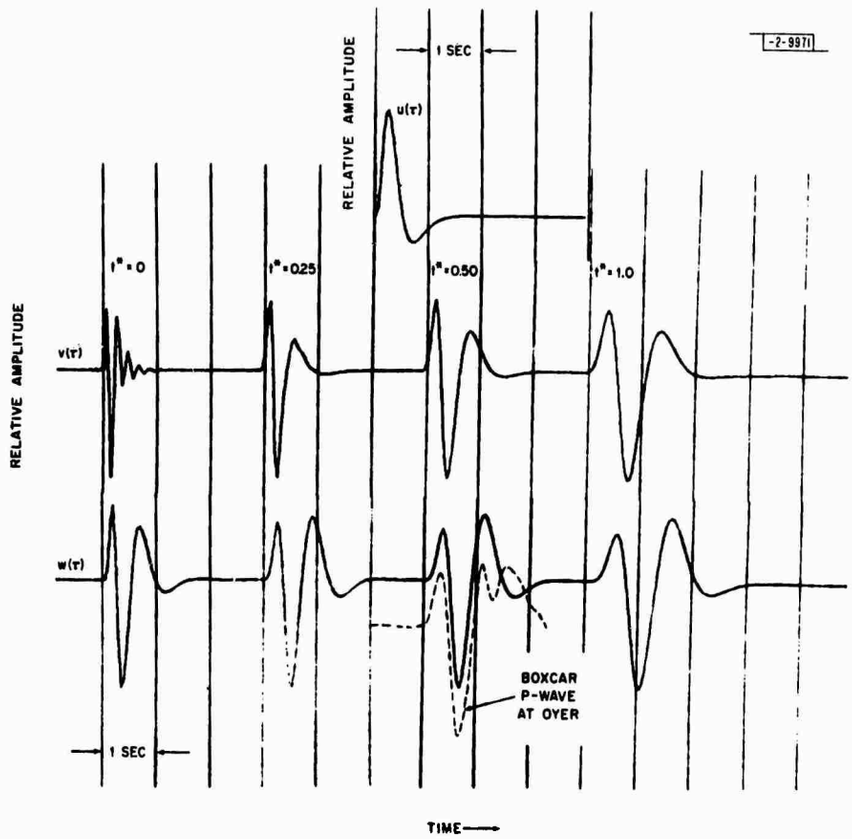

Fig. I-10. Synthetic teleseismic records far NTS shot Boxcar. The displacement source function in the far field, $u(\tau)$, is obtained by scaling up Haskell's reduced displacement potential for Hardhot. The middle row of traces, $v(\tau)$, shows the combined response of the Earth's attenuation, recording seismometer and anti-aliasing filter. The bottom row, $w(\tau)$, shows the convolution of the source with each response in the middle row. Superposed is the P-wave recorded at Oyer from Boxcar.

BLANK PAGE

II. PROPAGATION PATH

A. BODY WAVE SHADOWS FOR LONGSHOT

As has been discussed in previous SATS (30 June 1970, DDC AD-710613 and 31 December 1970, DDC AD-718971), inhomogeneities in the mantle would be expected to focus and defocus seismic ray paths, producing relatively systematic errors in observed body-wave magnitudes. For large events, for which a great number of observations are available, such systematic errors will tend to be reduced in the process of taking an average. However, for small events which are recorded at only a small number of high-quality stations, the resulting errors can be quite large, and it is important to be able to predict and correct for them.

The most pronounced known lateral variations in the mantle occur beneath island arcs. The nuclear explosion Longshot in the Aleutians provides an excellent opportunity to study this problem. Evidence has already been presented (SATS, 30 June 1970) of a pronounced short period P-wave shadow from Longshot, particularly in western Canada and southern Europe. Using three-dimensional ray tracing techniques,[1] we have found that a fairly accurate prediction of the location of this shadow can be obtained. The model used is two-dimensional and has a dipping lithospheric slab whose position is determined from the locations of earthquakes provided by Dr. E. R. Engdahl* and whose velocity contrast (maximum: 0.8 km/sec) is derived from observed travel-time anomalies.[2] Ray paths and wavefronts in a north-south cross-section (perpendicular to the island arc) are shown in Fig. II-1. The large shadow and region of multiple arrivals produced by the slab are obvious. Similar phenomena are exhibited by rays in other azimuths which pass near the slab, but the situation is complicated by the fact that rays do not lie in a plane and azimuth is not preserved along rays. Figure II-2 shows the points of emergence of a large number of rays, spaced 1° apart in angle of incidence at the source and at various azimuths. As can be seen, the predicted location of the shadow zone agrees remarkably well with that actually observed. The only large discrepancy occurs for eastern Canada and the northeastern United States; the data give no indication of a shadow, though one is predicted. We have calculated the average magnitudes in the shadow and the insonified region using values from the World-Wide Standard Seismographic Network, the Canadian Network, the Long Range Seismic Measurements Network and the United Kingdom arrays. Values reported by Lambert, et al.,[3] were used, excluding those reported as dubious and those near the predicted shadow boundary. The average value found outside the predicted shadow is 5.98 ± 0.34 (52 values), while inside it is 5.49 ± 0.58 (16 values). If the 4 values for eastern Canada and the northeastern U.S. are excluded, the value in the shadow becomes 5.21 ± 0.38.

Thus the structure beneath the Aleutians produces an anomaly approaching one unit in body wave magnitude and the geographic distribution of this anomaly can be predicted reasonably well from a simple two-dimensional model based on earthquake locations and travel-time anomalies. This result raises the possibility of calibrating various source regions and considerably improving magnitude measurements, especially for small events.

B. R. Julian
D. Davies

---

*Personal communication.

B. COMPARISON OF LOVE AND RAYLEIGH-WAVE MULTIPATH PROPAGATION AT LASA

In a recent paper, Capon[4] analyzed the multipath propagation of fundamental-mode Rayleigh waves at LASA. This measurement provided both angle of arrival and group delays for the 20, 25, 33 and 40 sec period groups, so that reasonably good conjectures could be made about the actual propagation paths for these period groups during the 800 sec time interval following the onset time of the fundamental-mode Rayleigh wave. It was found that, in almost all cases for the 26 events which were analyzed, the propagation paths could be associated with refractions and reflections at the continental margins. The reflection of a group was found to take place usually at a continent-to-ocean boundary and the angle of incidence usually exceeded the critical angle for the period of the group.

The particle motion for Love waves is transverse to the direction of the propagation path. Thus, there will be a signal output, due to the Love wave, only on the horizontal seismometer which is oriented transverse to the direction of propagation. As yet, the Love wave has not been found to be as important as the Rayleigh wave for the purposes of seismic discrimination. The diagnostic capabilities of the Love wave may be about as good as those of the Rayleigh wave for discriminating between earthquakes and underground nuclear explosions. However, it is more difficult to observe Love waves on a horizontal seismometer at low surface-wave magnitudes than it is to see Rayleigh waves on a vertical seismometer. Although the signal for the Love wave is approximately the same as that for the Rayleigh wave, the noise power on the horizontal seismometers is usually more than 10 dB greater than that on the vertical seismometer.[5] This larger noise power level is apparently due to local ground tilting caused by atmospheric pressure fluctuations which affect the long-period horizontal seismometers but not the long-period vertical component.

Nevertheless, the analysis of Love waves is important for several reasons. One reason is that it is important to know how any possible multipath propagation of Love waves will contaminate the Rayleigh wave when observed on a horizontal seismometer oriented in the radial direction. Another reason is that the measured dispersion curves of Love waves can be used to determine crustal structure.[6] In addition, it is possible that the noise, due to local tilting of the earth's surface, on the long-period horizontal seismometers may be reduced. In this case the Love wave may play a much more important role in seismic discrimination.

The group and phase velocities of fundamental-mode Love waves for continental regions differ from those of oceanic regions,[7,8] so that the refraction, as well as reflection, of Love waves at continental margins will lead to complex propagation paths for these waves, as was the case also for Rayleigh waves.

An investigation has been made of the multipath propagation of Love waves using observations obtained from the LASA. These results have been compared with those obtained by Capon[4] for Rayleigh waves.

The high-resolution (HR) method, described in detail by Capon,[9] was used to measure the frequency-wavenumber spectrum over four successive nonoverlapping 200-sec intervals, starting at the onset time of the Love wave, so that a total of 800 sec was considered. The measurement was made at 0.025, 0.030, 0.040 and 0.050 cps corresponding to period groups of 40, 33, 25 and 20 sec, respectively. The details of the measurement are the same as given by Capon,[4]

with the only exception that the rotated long-period horizontal components are analyzed as well as the long-period vertical (LPZ) components. This particular aspect of the measurement will now be described.

The HR method is first applied to the array of LPZ components. This provides estimates of power and phase velocity at each frequency for the Rayleigh waves. The HR method is then applied to each array of long-period radial (LPR) and long-period transverse (LPT) components which are obtained by rotating the long-period east-west (LPEW) and long-period north-south (LPNS) components in the conventional manner. For each set containing appreciable Love and Rayleigh energy, two peaks will usually appear, one giving Love wave power contribution and phase velocity, and the other yielding the analogous horizontal Rayleigh wave estimates. The identification and separation of Love waves by this method may be obtained by matching horizontal Rayleigh-wave peaks one-to-one with those obtained from the LPZ components. The remaining peaks, therefore, represent Love wave contributions. This method is applicable if the propagation directions for Love and Rayleigh waves are sufficiently different so that the HR method can resolve separate peaks for each wave type. When the directions coincide, the phase velocity differences may not be sufficient for the HR method to resolve two distinct peaks. In this case we can still identify the different wave types as follows.

We assume that the Love and Rayleigh waves are propagating from azimuths of Θ_L and Θ_R, respectively, and that a transverse component is obtained from an azimuth of $\Theta_L + \Delta\Theta$, by rotating the LPEW and LPNS components. The azimuths Θ_L and Θ_R are assumed to be close enough in value so that the HR method provides only a single peak for both wave types using the LPT components. If Θ_R is equal to $\Theta_L + \Delta\Theta$ then, of course, there will be no contribution on the LPT components due to the Rayleigh wave. The amplitude of the Love wave may easily be shown to be

$$L = [T - R' \sin(\Theta_R - \Theta_L - \Delta\Theta)] \sec \Delta\Theta$$

where T is the transverse component obtained for the direction $\Theta_L + \Delta\Theta$ and R' is the amplitude of the Rayleigh wave. The above equation may be rewritten (for power measurements) as

$$20 \log L = 20 \log[T - R' \sin(\Theta_R - \Theta_L - \Delta\Theta)] + 20 \log \sec(\Delta\Theta)$$

It can be assumed that R' and Θ_R are known from HR analysis of the LPZ sensors on which we can obtain only pure Rayleigh motion. This assumes that the particle motion of the Rayleigh wave is retrograde circular so that the vertical component is equal to the radial component. Thus, the Love wave power, as measured using the LPT components, may be obtained by subtracting out the Rayleigh wave contribution as indicated above. If R' is small relative to T, or if $\Theta_R - \Theta_L - \Delta\Theta$ is small, say less than 10°, then the Rayleigh component may be neglected in computing the Love wave power. Hence, using the above procedure it is possible in almost all cases to identify the Love-wave component.

The trial-and-error procedure which was used to determine the propagation paths for Love waves is similar to that described previously for Rayleigh waves by Capon.[4] Two examples of such propagation paths are shown in Figs. II-1 and II-2 for both the Love and Rayleigh wave of an event. The timing sequence for the group arrivals is not shown in any of these figures. Any

two propagation paths whose azimuthal angles of arrival at LASA are within 3° of each other are usually merged into a single path. In addition, all propagation paths in these figures are drawn as straight-line segments. All refractions and reflections are depicted as taking place at the geographic boundaries for the continents although it is more likely to take place at the continental margins. The difference is in most cases small and will be neglected. Only one refraction or reflection is taken into account on each epicenter-to-LASA path.

The propagation paths for the 21 November 1966 Kurile Islands event are shown in Fig. II-3. We see that initially, for both Love and Rayleigh waves, the longer-period groups arrive at LASA along the great circle path between LASA and the epicenter, or slightly refracted versions of this path. These groups are followed by shorter-period groups which are refracted and reflected at the continental margin. In addition, the multipath propagation of the Love waves is strikingly similar to that of the Rayleigh waves. However, the two sets of paths are sufficiently different from each other that it would be difficult to predict one set from the other, except for the gross details. These conclusions are also brought out by the propagation paths depicted in Fig. II-4.

We observe that reflection of a Love-wave group usually takes place at a continent-to-ocean boundary and that the angle of incidence often exceeds the critical angle for the period of the group. This result is to be expected, since it is at these angles of incidence that reflection of large amounts of energy would be expected. A similar result has been found for Rayleigh waves by Capon.[4]

J. Capon

C. CODA COHERENCE – A DISTINCTION BETWEEN DIFFERENT MANTLE REGIONS

The signal following the arrival of a short period P-wave has a variety of origins. If the event is an explosion we can assume that there is relatively little activity at the source beyond 5 sec after the time of detonation. Rayleigh waves from an explosion are well known to be small in amplitude, but there is the possibility that they be converted to P-waves on encountering obstacles. Energy arguments based on observed surface waves from explosions rule out this as a major contributor to coda. Reflections from discontinuities in the Upper mantle either at source or receiver of type pdpP are a major contribution[10] and conversion of P-waves to Rayleigh waves near the receiver can also produce coda, although this latter can be identified and suppressed by an array. One remaining source of coda is scattering due to heterogeneity in the mantle. This is a subject about which little is known at present; but recent results from LASA, that are presented here, may make a new contribution.

Figure II-5 displays seismograms from the five innermost subarrays of LASA – the B ring and A0. A presumed explosion from the Caspian Sea region is shown, and the seismograms have been placed in register on the first P-wave. For a period of more than 150 sec the five traces show a high degree of coherence. We note, in particular, that there is very little signal which could be attributed to P-Rayleigh conversion at LASA in that this signal would be incoherent from subarray to subarray and would be strongest immediately following the P-wave, where in fact the traces bear a close similarity to one another. We have already concluded[10] that the origin of this coherent signal is internally reflected P-waves in the Upper Mantle of the source region.

Figure II-6 is a display of identical seismometers, but this time the signal is from a presumed explosion in Eastern Kazakh. The amplitude of the first P-wave in Figs. II-5 and II-6 has been made the same and it is clear that the coda is utterly different between the two events. The complete incoherence across an aperture of only 20 kms cannot be explained by any sub-LASA structure as it would have manifested itself for the Caspian event also, which approached LASA at a similar dip angle and an azimuth different only by 20°. The problem is that while it is necessary to ascribe the origin of this incoherence to a region nearer the source than the receiver, the closeness of the sensors in the A and B rings requires that any scattering radiator under the Eastern Kazakh region must be producing signal of extreme variability with receiver position. An example will illustrate further, and we chose two new events in the same regions in order to establish the principle more generally. Figure II-7 is a linear array of seismometers approximately oriented toward another Caspian event. These instruments are selected from subarrays A0 and B4 and the typical spacing is 1 to 2 km between adjacent instruments. In Fig. II-8 the same seismometers are displayed for another Kazakh event. The Caspian event again acts as a control on how much of the incoherence of the coda can be of near receiver origin. The differences between Figs. II-7 and II-8 are large even within the smaller array. Some features in Fig. II-8 persist across the small array, but in general there are 'highlights' which do not persist over an aperture of more than 2 or 4 kms, in strong contrast to Fig. II-7. Thus in addition to some pdpP signal there is a large random constituent. There seems only one way, at the present, of explaining this signal, and that is in terms of interference between scattered waves producing a complicated pattern near the receiver. We define a seismic 'halo' in Sec. III and Fig. II-9 shows the sort of ray paths involved. I propose that the region beneath Eastern Kazakh has a strong degree of lateral heterogeneity producing this halo. At what depth the scattering occurs we, as yet, don't know.

D. Davies

D. WAVE PROPAGATION IN TRANSITION LAYERS

An interesting problem in seismic wave propagation is the reflection of plane waves off transition zones in which velocity and density vary smoothly with depth. An approximate solution is obtained by dividing the inhomogeneous transition zone into a lamination of many thin homogeneous layers. Using the Thomson-Haskell method[11,12] the reflection response can be tabulated over a window of frequencies ω and numerically inverted back to the time domain.

Two drawbacks of this method are that an iteration through all the layers is required for each frequency tabulated, and at high frequencies, considerable round off errors may accumulate due to products of exponential terms in ω occurring in the layer iteration.

An approximate time domain solution for homogeneous P- and SV-waves has been developed[13] which avoids the above difficulties in the Thomson-Haskell method. At vertical incidence, for example, the transition layer is divided into many homogeneous layers with one-way travel times $\Delta\tau/2$. In this way an incident compressional wave pulse is multiply reflected from the various interfaces between layers, giving a reflection response which is a converging time series sampled every $\Delta\tau$ seconds.

A single matrix iteration through all the layers gives a reflection response of the form

$$R_{pp}(z) = f(z)/g(z) \qquad \text{(II-1)}$$

where f(z) and g(z) are polynomials with real coefficients in the Fourier transform variable

$$z = e^{-i\omega\Delta\tau} \quad . \tag{II-2}$$

The use of the z-transform eliminates any explicit calculations in ω and demonstrates the scattering of the waves in time. In Eq. (II-1), polynomial division of f(z) by g(z) generates the converging series

$$R_{pp}(z) = r_o + r_1 z + r_2 z^2 + \ldots \quad .$$

Since z^n represents a delay in time of $n\Delta\tau$ sec, the infinite series above can be inverted by inspection to yield the time series

$$R_{pp}(t) = r_o\delta(t) + r_1\delta(t - \Delta\tau) + r_2\delta(t - 2\Delta\tau) + \ldots \quad . \tag{II-3}$$

Each coefficient r_n represents the area of the pulse arriving at time $n\Delta\tau$. In order to convert these areas to amplitude, $R_{pp}(t)$ is divided by $\Delta\tau$. This allows us to compare approximate solutions for various $\Delta\tau$. For small $\Delta\tau$, such solutions can also be compared with continuous time solutions obtained by other methods.

The first example considered is a linear transition zone in compressional velocity between two homogeneous half spaces, with constant density everywhere. The continuous velocity and density profiles are shown in Fig. II-10. Superposed on the transition zone are three sets of homogeneous layers used to approximate the linear velocity gradient. The two-way travel times for the layers within each set are $\Delta\tau$ = 0.4, 0.2 and 0.1 sec, respectively.

The reflection response of each set of layers is shown in Fig. II-11 for an incident delta function source of compressional particle velocity. As $\Delta\tau$ decreases, the reflection response quickly converges to a slightly tapered boxcar function of amplitude 0.25 and width $\simeq$ 1.4 sec.

Also displayed is the approximate reflection response obtained in close form by Richards[14] using a propagator matrix technique in the frequency domain. His method can treat linear gradients in density or velocity but is approximate in that only terms of order O(1) and O(1/ω) are considered. Thus Richards' solution represents a high frequency approximation which is excellent for this particular model, which has no density gradient. In the frequency domain both solutions match almost perfectly the exact response given by Berryman, et al.[15]

The second example is a model of the core-mantle boundary in which both velocity and density rapidly change over a short depth. (This is only to be considered as an example for calculation purposes – not a model based on present data). No exact solution exists for such a problem. We consider a transition zone 5 km thick with velocity and density profiles shown in Fig. II-12. Two time increments $\Delta\tau$ = 0.1 and 0.05 were used to calculate the reflection response for an incident compressional source in the mantle. These responses are shown in Fig. II-13 and differ only in the resolution of the first motion. The theoretical two-way travel time through the transition zone is T = 0.932, at which time the second jump occurs in the approximate solutions.

Although the major advantage of this technique is the rapid calculation of time domain responses, the frequency response is easily obtained from Eq. (II-1). The real coefficients of the

f(z) and g(z) are finite length time series. Taking the spectral ratio of the two time series gives $R_{p\rho}(\omega)$ for frequencies in the range

$$\frac{-\pi}{\Delta\tau} \leqslant \omega \leqslant \frac{\pi}{\Delta\tau} \quad .$$

Thus for either time or frequency domain responses only one iteration through the layers is required.

This method is applicable for homogeneous waves at non-normal incidence and is being used to study the effect of the core-mantle boundary on incident waves of arbitrary shape.

C. Frasier

REFERENCES

1. B.R. Julian, "Ray Tracing in Arbitrarily Heterogeneous Media," Technical Note 1970-45, Lincoln Laboratory, M.I.T. (31 December 1970), DDC AD-720795.
2. D. Davies and D.P. McKenzie, "Seismic Travel-Time Residuals and Plates," Geophys. J. 18, 51-63 (1969).
3. D.G. Lambert, D.H. von Seggern, S.S. Alexander and G.A. Galat, "The Long Shot Experiment," Seismic Data Laboratory Report No. 234, Arlington, Virginia (1970).
4. J. Capon, "Analysis of Rayleigh-Wave Multipath Propagation at LASA," Bull. Seismol. Soc. Am. 60, 1701-1731 (1970), DDC AD-716084.
5. J. Capon, "Investigation of Long-Period Noise at the Large Aperture Seismic Array," J. Geophys. Res. 74, 3182-3194 (1969).
6. K. Aki and K. Kaminuma, "Phase Velocity of Love Waves in Japan – Part 1. Love Waves from the Aleutian Shock of March 9, 1957," Bull. Earthq. Res. Inst. 41, 243-259 (1963).
7. J. Oliver, "A Summary of Observed Seismic Surface Wave Dispersion," Bull. Seismol. Soc. Am. 52, 81-86 (1962).
8. J. Brune, "Surface Waves and Crustal Structure," in The Earth's Crust and Upper Mantle, P.J. Hart, editor (American Geophysical Union, Washington, D.C., 1969), pp. 230-242.
9. J. Capon, "High-Resolution Frequency-Wavenumber Spectrum Analysis," Proc. IEEE 57, 1408-1418 (1969), DDC AD-696880.
10. D. Davies, E.J. Kelly and J.R. Filson, "The Vespa Process for the Analysis of Seismic Signals," Nature 232, 8-13 (1970).
11. W.T. Thomson, "Transmission of Elastic Waves Through a Stratified Solid Medium," J. Appl. Phys. 21, 89-93 (1950).
12. N.A. Haskell, "The Dispersion of Surface Waves on Multilayered Media," Bull. Seismol. Soc. Am. 43, 17-34 (1953).
13. C.W. Frasier, "Discrete Time Solution of Plane P-SV Waves in a Plane Layered Medium," Geophysics 35, 197-219 (1970).
14. P.G. Richards, "Elastic Wave Solutions in Stratified Media" (submitted to Geophysics) (1971).
15. L.H. Berryman, P.L. Goupillaud and K.H. Waters, "Reflections from Multiple Transition Layers – Part 1. Theoretical Results," Geophysics 23, 223-243 (1968).

Sectian II

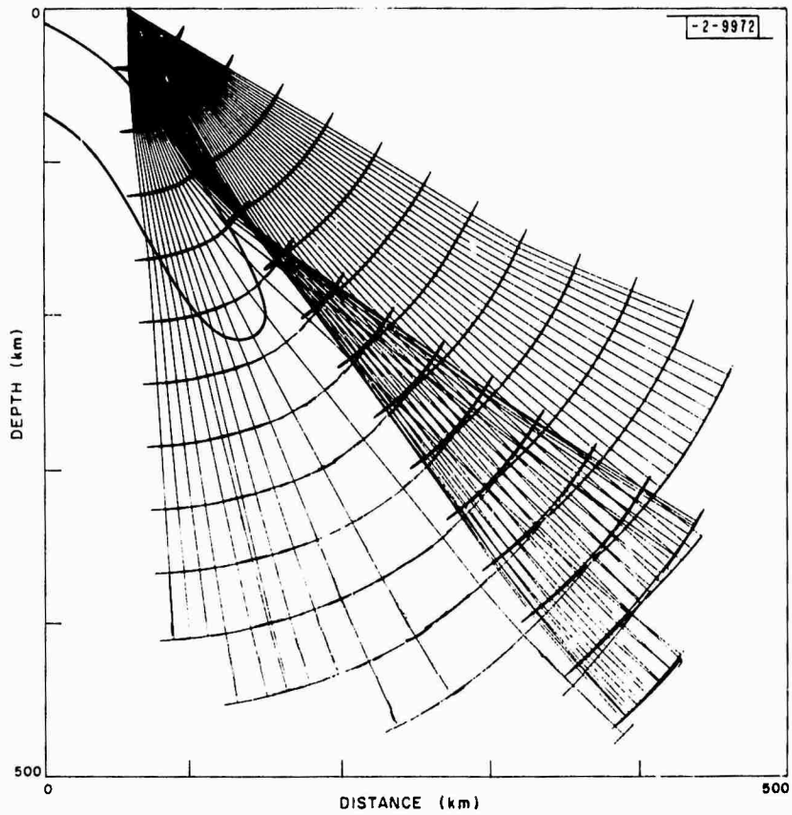

Fig. II-1. P-wave ray paths thraugh Aleutian slab model. A narth-sauth sectian perpendicular to the island arc is shown, with rays spaced 1° apart at the facus. Wave frants are drawn at 5 sec intervals.

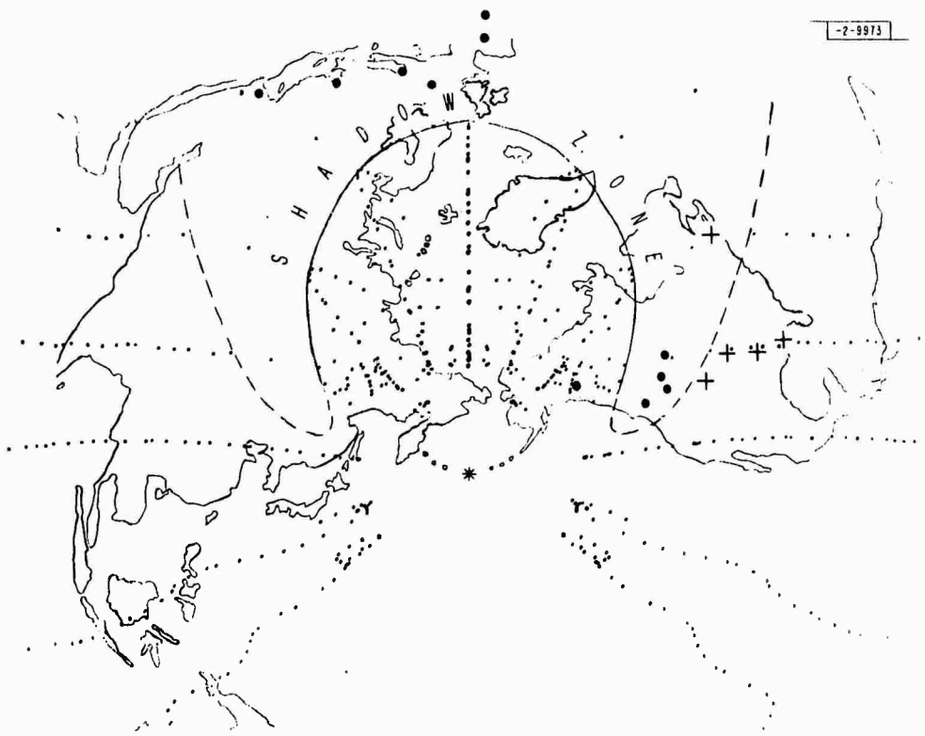

Fig. II-2. Calculated points of emergence of P-waves (small dots) from Longshot. Angles of emergence at source are spaced 1° apart, and launch azimuths of 0°, 20°, 40°, 60°, 70°, 80°, 100° and 120° are used. Rays in the fully insonified region to the south have been eliminated. A general outline of the world is given in azimuthal equal area projection on Longshot, and stations (north of Longshat) reporting magnitudes less than 5.4, or greater than 6.4, are represented by large dots and crosses, respectively.

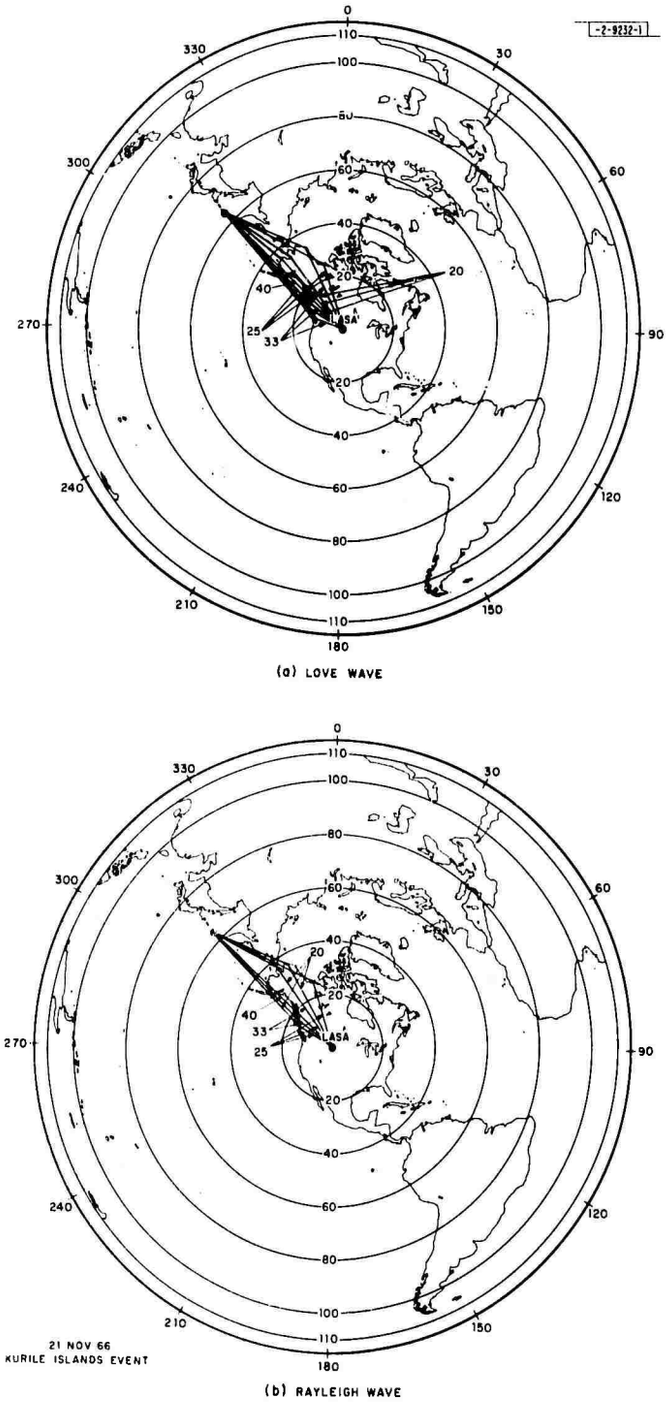

Fig. II-3. Propagation paths for the Love and Rayleigh waves of the 21 November 1966 Kurile Islands event.

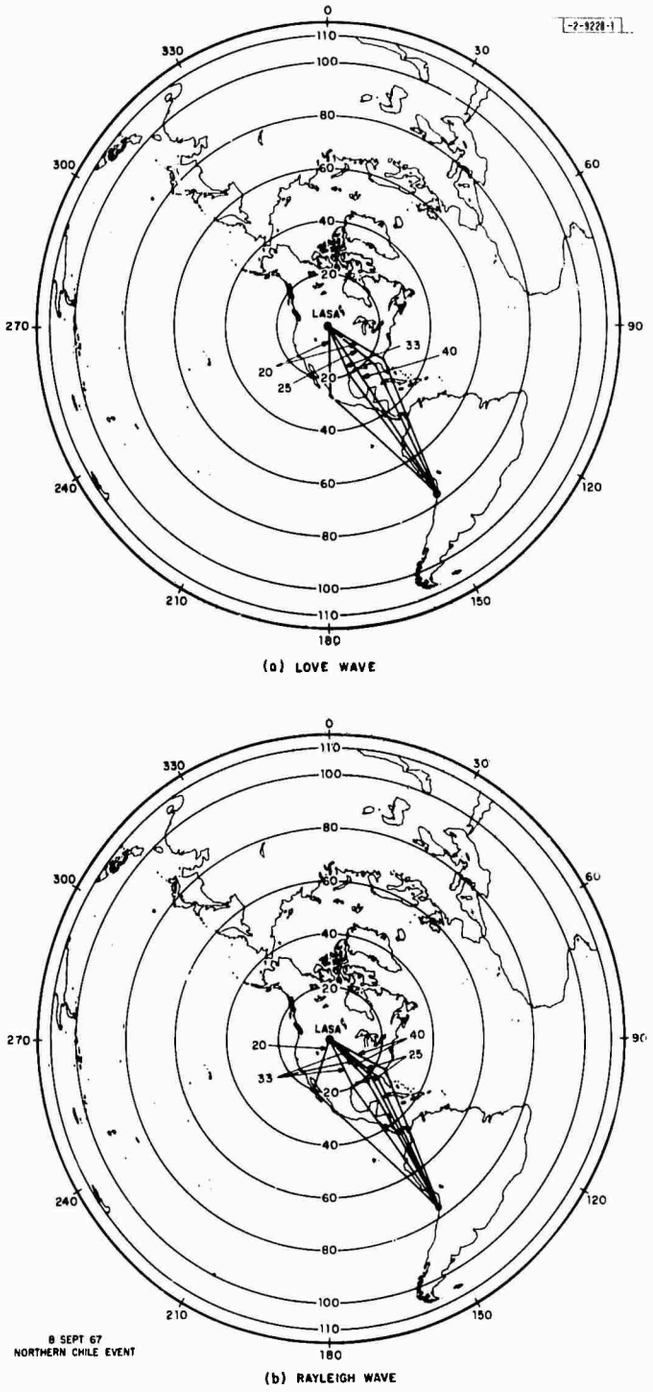

Fig. II-4. Propagation paths for the Love and Rayleigh waves of the 8 September 1967 Northern Chile event.

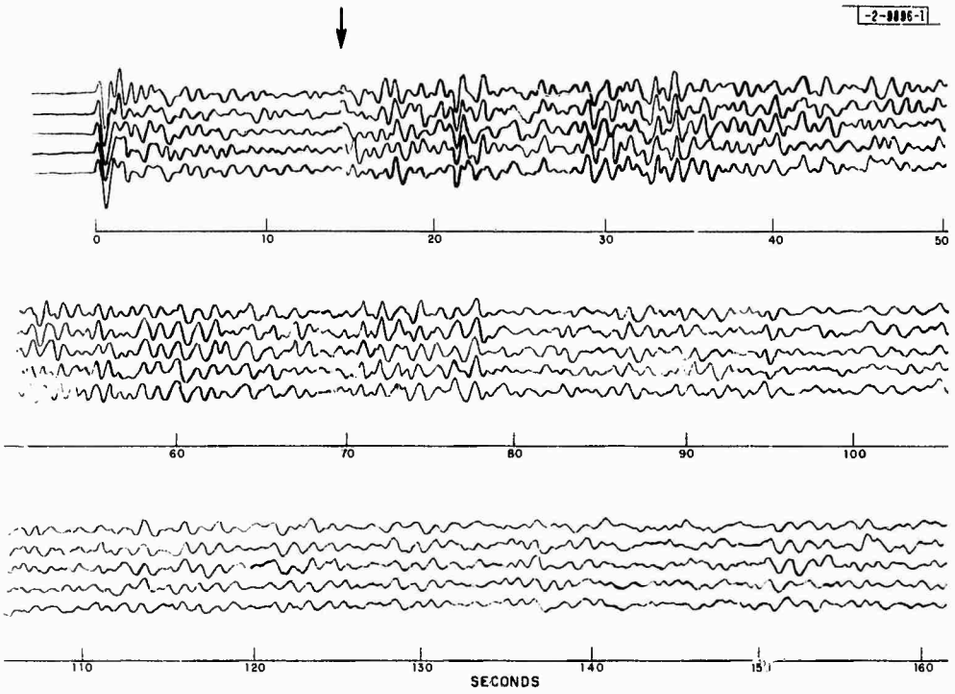

Fig. II-5. Seismic signal (short period sensors) from an event in the Caspian Sea region. The five innermost subarrays are displayed in register. The gain is raised at the vertical arrow.

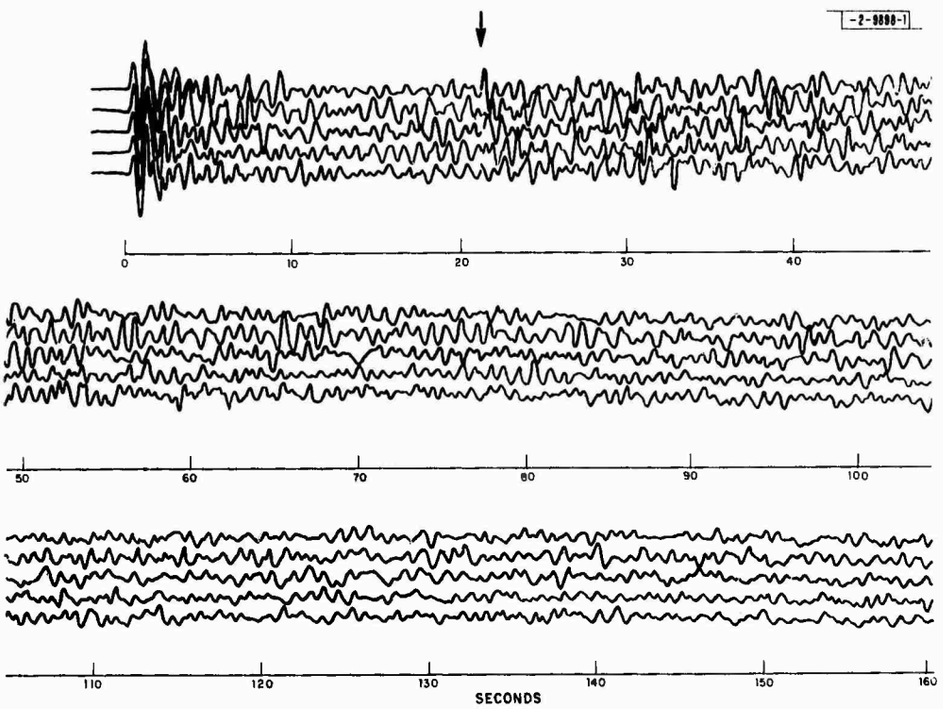

Fig. II-6. An Eastern Kazakh event; the layout is identical to that for Fig. II-5.

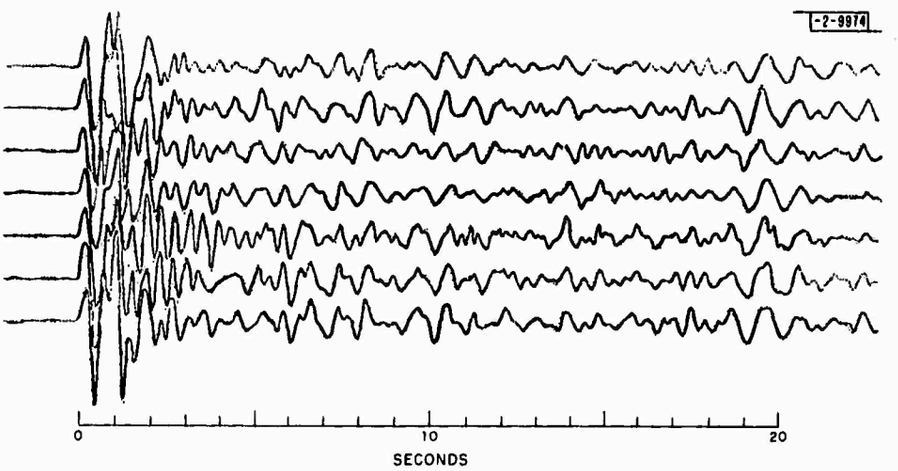

Fig. II-7. Seismic signal from a small linear array oriented N-S to receive a Caspian Sea event. The data is registered an the P-wave. Individual sensors are 1 to 2 km apart.

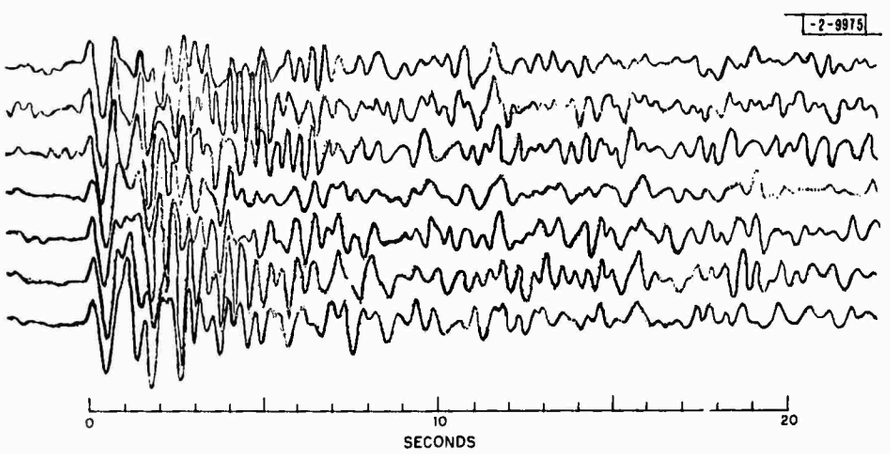

Fig. II-8. An Eastern Kazakh event; the loyout is identical ta that af Fig. II-7.

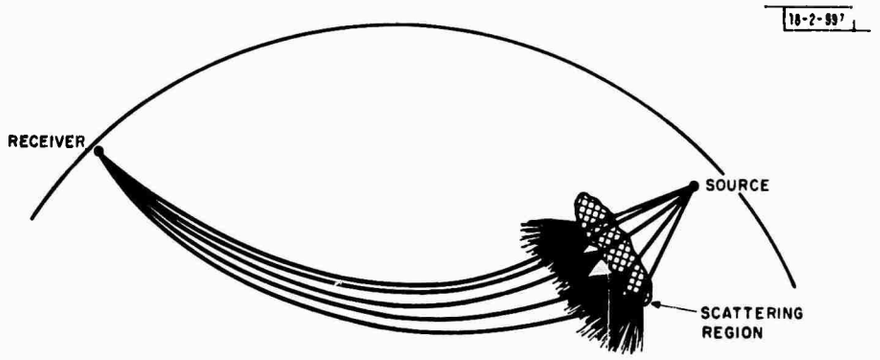

Fig. II-9. Possible contributions to o seismic "holo".

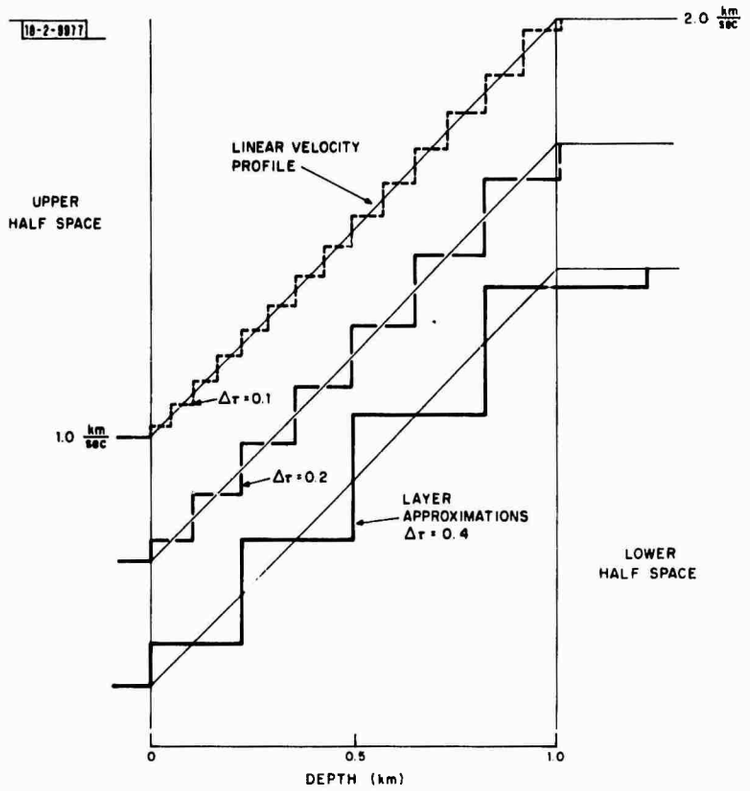

Fig. II-10. Approximotion of o lineor tronsition zone in velocity by lominotions of equol time, homogeneous loyers. Three sets of loyers ore shown for two-woy trovel times $\Delta\tau = 0.4$, 0.2 ond 0.1 sec through the individual loyers.

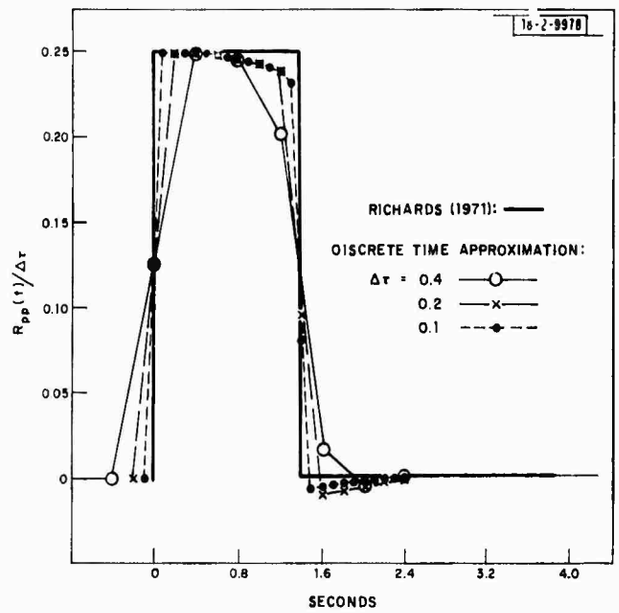

Fig. II-11. Reflection response $R_{pp}(t)/\Delta\tau$ for the three sets of layers in Fig. II-1 for an incident delta function of velocity from above. Also shown is the continuous time solution obtained by P.G. Richards, which is accurate to $0(1/\omega)$ in the frequency domain.

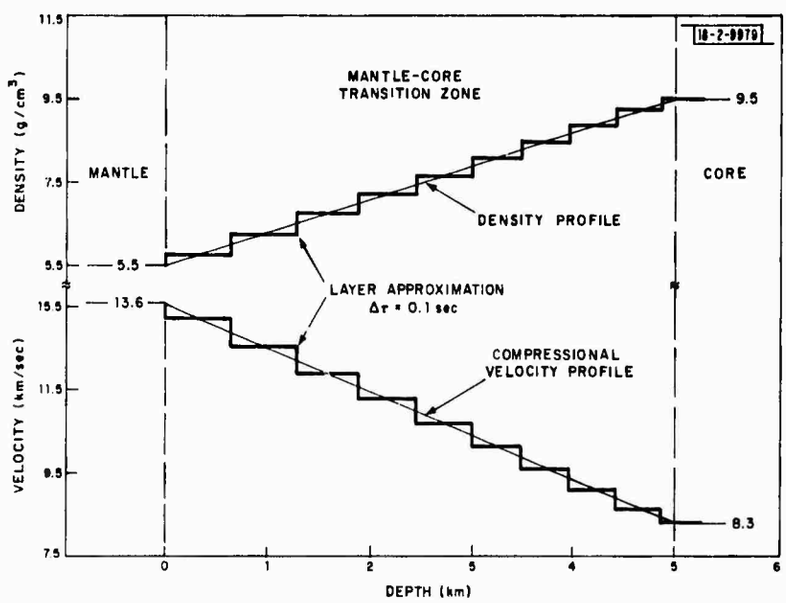

Fig. II-12. Approximation of the mantle-core boundary of the Earth by a lamination of equal time layers for $\Delta\tau$ = 0.1 sec. Both density and compressional velocity are assumed to be linear over a transition zone of 5 km.

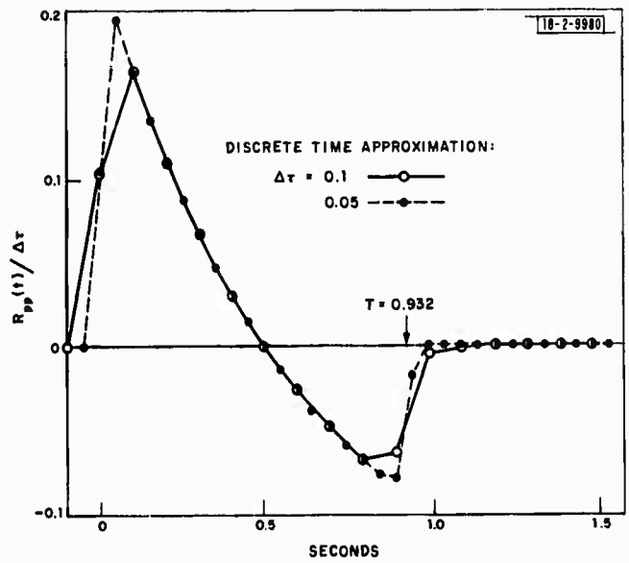

Fig. II-13. Reflection response $R_{pp}(t)/\Delta\tau$ for a delta function of particle velocity incident to the mantle-core boundary from above. Two sets of layers were used, i.e., $\Delta\tau = 0.1$ and 0.05 sec. The coarser set is shown in Fig. II-12.

BLANK PAGE

III. RECEIVER AND DATA PROCESSING SCHEMES

A. NORSAR TIME ANOMALIES

An evaluation of the NORSAR travel time anomalies is being undertaken with the aim of producing some preliminary values for the NORSAR station corrections. Data used in the investigation were obtained from the operation of the interim NORSAR during early 1970. During the interim operation only the center seismometer of each of 18 subarrays was recorded on magnetic tape. From the more than 600 events that were processed during this period, only 206 were found to be acceptable for this study. All of these 206 events were located by USCGS and were recorded on 15 or more NORSAR seismometers. The moveouts or lag times for these events were first determined by the cross-correlation output of the event processor at NORSAR. Each event was later inspected by an analyst to ensure the accuracy of the data.

This information was then used to compute the azimuth and horizontal phase velocity by the plane wave approximation to the wave front. As was expected, the difference between the computed azimuth and the true azimuth was often large. However, the behavior of the azimuth error was quite unexpected. Figure III-1 shows the NORSAR P-wave zone of the world in an azimuthal equidistant projection centered on NORSAR. From the azimuth error plot in Fig. III-2, it can be said that the azimuth error is not a simple function of azimuth alone, as was the case for LASA. The error at NORSAR varies quite drastically with small changes in event location. For example, while there is practically no azimuth error for events from the Aleutian Arc, the error reaches a maximum value for events from southern Honshu and the Ryukyu Islands. Here, the measured azimuth is about 8° greater than the true azimuth. Another region of large change is the azimuth between South America and Central America. Here, the azimuth error seems to vary by as much as 10° or more over an azimuth change of only about 30°. While data from this region are sparse, if the interim NORSAR data are an indication of the azimuth errors made by the full NORSAR, then the azimuth errors observed here are the greatest ever observed on any large array, LASA or the TFSO extended array.

The error made in the horizontal phase velocity does not seem to vary as drastically as the azimuth errors. From Fig. III-3 it seems that for small distances the velocity errors are small and are both a function of distance and azimuth. At distances that approach the core grazing angle, the velocity error does become rather large in addition to splitting into two distinct groups. The separation of data into these two groups is associated with two seismic zones which are almost 180° apart. Here, as with the azimuth errors, the region from South America to Central America exhibits the largest anomaly. At this time it is difficult to suggest any geological feature at NORSAR which may cause such sizeable errors in both azimuth and velocity, so source region heterogeneities, such as were discussed in SATS (30 June 1970 DDC AD-710613), will have to be invoked.

A study of the individual station errors in travel time has shown surprising results. Using the seismometer from subarray 4C as the reference, the measured arrival times at each subarray were compared to the computed arrival times. Subarray 4C was chosen as the reference subarray because it recorded more of the events than did any other subarray. The delay anomaly is defined as:

$$A_i = O_i - O_{4C} - T_i + T_{4C}$$

where

O = observed arrival time at the subarray

T = computed arrival time at the subarray based on USCGS epicenter and Jeffreys-Bullen (J-B) Tables.

Figure III-4 is typical of the time anomaly found for most of the subarrays. From this figure and Fig. III-5 it seems apparent that the station error is more a function of distance than azimuth. However, since this trend is seen at most of the subarrays it may be an error from the reference site 4C that is being imposed on the array. Further investigation into these effects is necessary before reaching conclusions as to their causes.

Data collected during the interim operation of NORSAR are providing a good data base for predicting station anomalies and plane wave errors. They also indicate that a good selection of events from all azimuths and distances will be necessary for a proper treatment of the NORSAR station corrections and array anomaly. Regions where the anomalies undergo the most rapid changes should be of particular interest when collecting data.

R. M. Sheppard

B. SHORT PERIOD SPECTRAL PROCESSING

Variations in the spectral content of signals within an array were discussed in our last SATS (31 December 1970, DDC AD-718971). It was indicated that the average spectra from sensors (spectraforms) as well as the spectra of beams should be considered for discrimination and scientific studies. Modifications and additions to the Lincoln Laboratory Data Analysis Console have now been completed which allow one to obtain conveniently, and save on magnetic tape, spectraforms, beam spectra, and short sections of data for up to thirty-two channels of data. More than fifty successful runs have been completed using these programs. The purposes of the runs were varied and included several different types of data from different arrays. Detailed analysis and interpretation of results has just begun.

The short period P-wave spectra of four presumed nuclear tests from Eastern Kazakh and ten earthquakes recorded at NORSAR during the interim period have been studied. NORSAR data during that period consisted of one short period sensor from each subarray site sampled at ten samples per sec. Typically there were fifteen good channels per event and 5 sec of data were used to obtain spectra. The epicentral distances of the earthquakes used are between 18° and 80°. All the earthquakes and presumed explosions are in the body-wave magnitude range of 4.9 to 5.9 as reported by USCGS. The spectrum of the best beam which was formed using "eye-ball" time picks and the average spectrum of each event have been computed. Based on the beam spectra and the average spectra of these fourteen events, the following observations are made:

(1) The beam spectra are smaller than the average spectra in all cases. The beamforming loss is a function of frequency as well as epicentral distance, as can be seen on Fig. III-6 which was constructed using data from four of the events. The data shown have been selected to include only measurements with good signal-to-noise ratios. The

ratio of the average spectra and beam spectra is an increasing function of frequency. The loss of high frequencies in beamforming is more severe at intermediate epicentral distances ($\Delta \simeq 40°$) than at small and large distances although in all cases the spectral peak is in the 1.0 to 2.0 cps band and the beamforming loss at the peak frequency is 3 dB.

(2) The frequency band over which signal-to-noise ratios are satisfactory is very comparable for spectraforming and beam spectra. The noise reduction of beamforming is almost entirely negated by the loss of signal at high frequencies. However, unless some future development mitigates in favor of spectraforms, it is probably not to be preferred over beamforming since it is at least an order of magnitude more demanding computationally.

(3) There is a significant difference in the band width of the presumed explosion's spectra and the earthquake's spectra as seen through the uncorrected NORSAR instruments. For example, the −10 dB spectral width of all of the four presumed explosions is between 3 and 4 cps, whereas it is between 1 and 1.6 cps for all of the earthquakes. This simple discriminant, which currently has no physical justification, may well fail when applied to explosions from other areas of the world or to a larger suite of earthquakes. This is a topic for future research.

In the SATS of December 1970, we also introduced a new (ALPHA-C) spectral estimation technique. In addition to testing simple spectraforms we have obtained the average spectra of three small magnitude events recorded at NORSAR. A gain of 2 to 5 dB over the simple spectraforming technique is obtained through the application of this method. This is encouraging although it is still not clear that the computational load can be justified when compared to simple beamforming.

Among the ten earthquakes processed there is one from Western Iran which peaks at a much higher frequency than the rest of the earthquakes. This peculiarity motivated the study of the spectra of a group of six other earthquakes from the same area. These were recorded on the 20 km Oyer subarray installed as part of the preliminary noise studies at NORSAR. Both beams and spectraforms were used. Interim NORSAR data for other events from the region were not available. Two of the events are from almost exactly the same epicenter as the first, are about the same size, and have very similiar short period spectra. The other four events are up to 4° from the original epicenter and have spectra which peak at somewhat lower frequencies. However those events also tend to have more energy. Since all of these events are associated with the Zagros thrust zone, it is likely they do have similiar mechanisms and we are in fact observing a scaling effect with the size of the event.

Most other beam spectra and spectraforms have been obtained as part of a program to investigate spectral scaling laws for both earthquakes and explosions. These include: (1) LASA data for six closely located deep events in South America; (2) LASA and Oyer data for four presumed Eastern Kazakh explosions and LASA data for seven additional Eastern Kazakh events; (3) LASA and Oyer data for a suite of nine events from the Aegean Sea plus an additional four recorded at LASA only. Analysis of these data from small but homogeneous suites of events has just begun and no results are yet available.

R. T. Lacoss
M. Mohajeri

C. PATTERN RECOGNITION TECHNIQUES FOR THE INTERPRETATION OF VESPAGRAMS AND BEAMSPLIT DATA

The VESPA (Velocity Spectral Analysis) and Beamsplit programs have been found to be useful as tools for geophysical research. This research has been concerned, to a great extent, with the identification of seismic phases on the basis of arrival time, velocity and direction of approach at LASA. VESPA is described in the 30 June 1968 (DDC AD-673354) and 31 December 1968 (DDC AD-682297) SATS. It will be recalled that in this program the LASA is steered to an appropriate azimuth and 61 beams are formed with slowness ranging from 0.0 to 12.0 sec/deg in increments of 0.2 sec/deg. The powers of each of the beams are computed over 1 sec intervals and contoured, in dB relative to the maximum power, as a function of time and slowness. In the Beamsplit program (SATS June 1967, DDC AD-657327) an appropriate time interval is chosen, usually about 3 sec long, and a square array (11 × 11) of beams is formed, uniformly separated by a specified distance (in the example we consider, 220 km). The power in each of the beams is computed over the 3 sec time interval and these powers are contoured as a function of latitude and longitude.

In both the VESPA and Beamsplit displays the analyst is presented with a contour plot in which there are a relatively large number of peaks and troughs. The problem of deciding which of these peaks is due to a seismic phase and is not caused by extraneous background, or signal-generated, noise is of prime importance in the interpretation of these data. This problem has been considered as one of testing multiple hypotheses, or statistical pattern recognition. A brief discussion of the results will now be presented, along with some actual applications in identifying certain seismic phases.

We are interested in detecting a signal in the presence of noise, at a particular time, using either the Beamsplit or VESPA. For simplicity, and with no loss of generality, we consider only the VESPA display (Vespagram). This problem can be considered as one in statistical pattern recognition, or testing multiple hypotheses.

The null hypothesis is:

H_o : Noise alone is present on the Vespagram,

and the alternative hypothesis is

H_j : Signal is present in noise on the Vespagram at slowness $\vec{\alpha}_j$.

The index j runs from 1 to N, where N is the number of independent beam outputs. That is, it is assumed that at a particular time there is only a single signal propagating across LASA and it has a slowness $\vec{\alpha}_j$, which is one of a set of discrete slownesses ranging from $\vec{\alpha}_1$ to $\vec{\alpha}_N$.

Let us first define noise and signal. The level of earth noise (microseisms) is usually well below that of the noise on the Vespagram in the period following a P-wave. This latter noise may have one of three origins:

(1) Signal converted near the array from P-waves to P-, S- and Rayleigh waves – incoherent across the aperture of LASA,

(2) The "seismic halo" – a generic term for P-waves which have been scattered en route from source to receiver and come into LASA as a largely coherent signal. However, at any one time there will be

many constituents of the halo of random phase and so this signal will appear complex (see Sec. II for further discussion of coherent/incoherent signals),

(3) Side lobes of the above.

On the other hand, the seismic signal is assumed to be:

(1) Well established phases,

(2) Phases specific to the source region such as the pdpP type phases described in the December 1970 SATS and in Davies, Kelly and Filson,[1]

(3) Clear large coherent signals from identifiable denumerable geophysical scattering or reflecting regions.

Let us pursue our halo analogy, and say that item (2) of the noise category would correspond to the water vapor halo around the moon; whereas, item (3) of the signal category would correspond to reflected moonlight from an artificial satellite.

Then, in order to determine a decision rule for deciding which hypothesis to choose on the basis of the observed data, or Vespagram, the following assumptions are made:

(1) The noise in the individual sensors of the array is signal-generated noise.

(2) The noise can be described as a Gaussian homogeneous random field whose frequency-wavenumber spectrum has a diffuse structure in wavenumber space.

(3) The power of a beam which is steered using the slowness $\vec{\alpha}_i$ is statistically independent of the power of any other beam with slowness $\vec{\alpha}_j$ provided $|\vec{\alpha}_i - \vec{\alpha}_j|$ exceeds the 3 dB slowness beamwidth of the LASA, $\vec{\alpha}_B$.

(4) The Vespagram surface, at a particular time, is discretely sampled in slowness with increment $\vec{\alpha}_B$, so that N statistically independent beam powers are obtained at the slownesses $\vec{\alpha}_1, \ldots, \vec{\alpha}_N$.

It may be shown[2] that the probability density function of the beam power, under H_o, is chi-squared with 2 degrees of freedom, and under H_j is Rician with parameters determined by the beam pattern of LASA. The joint probability density functions of the beam powers may be obtained quite simply by multiplying individual density functions, because of assumption (4) concerning statistical independence of the beam powers. Thus, the likelihood ratio may be computed to determine the optimum Bayes decision rule which leads to a minimum total probability of error. Hence, it may be shown that the optimum decision rule is based on a matched filter, or cross-correlation, system. In this system the LASA beam pattern is shifted to the slowness $\vec{\alpha}_j$ and cross-correlated with the beam powers. The maximum value of these cross-correlations is noted as occurring for one of the possible slownesses $\vec{\alpha}_1, \ldots \vec{\alpha}_N$, say $\vec{\alpha}_i$. If this value exceeds a certain threshold, then the signal is said to be present at the slowness $\vec{\alpha}_i$, otherwise the signal is said to be absent.

The decision rule can be simplified considerably if we assume that the beam pattern is ideal in the sense that it is unity for zero slowness and equals zero for slownesses that exceed the 3 dB width of the natural LASA beam pattern. In this case the decision rule is implemented as indicated in Fig. III-7. The beam with the maximum power is noted as occurring at the slowness $\vec{\alpha}_i$, or equivalently, in the i^{th} channel. If this power exceeds a certain threshold then signal is said to be present at the slowness $\vec{\alpha}_i$, otherwise the signal is said to be absent. It should be noted that in the Vespagram the beam power outputs indicated in Fig. III-7 correspond

to the beam powers, at a particular time, for the various independent slowness values. The application of the results in Fig. III-7 to the Beamsplit display is apparent. In this case the beam powers are associated with the various independent beams located at various latitudes and longitudes. The effect of the non-ideal shape of the beam pattern may be taken into account qualitatively by requiring not only that the maximum power exceed a threshold, but that the beam powers resemble the beam pattern.

The threshold is, of course, determined by the allowable false alarm probability. This false alarm probability is shown in Fig. III-8 as a function of the threshold, in dB relative to average noise power, and various values of N, which is the number of statistically independent beams. The number of such beams is approximately thirty for VESPA and about $30\Delta^2$ for Beamsplit data, where Δ is the distance in degrees between beams. Thus, in the Vespagram, a peak may be said to represent a discrete seismic signal if it is at least 8 dB above the average background noise level. This noise level should be taken at a time just prior to the arrival time of the signal when it is known that no signal is present. Then the probability that a peak 8 dB above the noise average could be noise itself is about 0.05. If we use a beam spacing of 2 degrees in the Beamsplit program then a threshold of 9 dB above the average background noise level is required to obtain a false alarm probability of about 0.05. The results in Fig. III-8 show that it is important to take the number of independent beams into consideration when identifying peaks as associated with propagating seismic waves.

We now wish to describe the application of the results to actual data obtained with the Beamsplit program for a South West Russia event. In the P-wave coda of this event, the Vespagram process detected a peak which could not be associated with any known seismic phase. The $dT/d\Delta$ and azimuth for this peak were converted into a location on the Earth's surface and a grid of 11×11 beams spaced 220 km (2°) apart and centered on this location was contoured (Fig. III-9) by the Beamsplit process. Several preceding intervals were also contoured for the same location and a mean power level was determined for the noise by inspection of the plots. The maximum beam power in Fig. III-9, which occurs at 68.0°N and 15.0°E, is about 9 dB above this average background noise level. At this threshold, we see from Fig. III-8 that the false alarm probability is about 0.05. Thus, we can identify this peak with a P-wave signal from the aforementioned region.

We can say more than this, however. The false alarm probability quoted is undoubtedly very conservatively high. Figure III-10 shows the theoretical array response to a signal coming from this region. Comparison of Fig. III-10 with Fig. III-9 clearly demonstrates that the general pattern of the theoretical and observed response are closely similar. This similarity could be quantified if required. Finally, the signal is geophysically reasonable. The region of its source is on the Norwegian continental margin which has a steep gradient and whose strike is perpendicular to the great circle from South West Russia to LASA. Thus P-waves arriving in this region from South West Russia would be reflected into a new $dT/d\Delta$ but retain their azimuth. The time of arrival of this signal is close to that for a signal which we call PP – P, where PP from South West Russia to Norway is converted (the dash represents this) into a P-wave with a new $dT/d\Delta$ which ends at LASA.

A recent paper[1] discusses this event in somewhat more detail.

J. Capon
D. Davies

D. CRUSTAL STRUCTURE BENEATH LASA FROM LONG-PERIOD P-WAVE SPECTRA

The response of a crustal model of parallel plane layers of homogeneous isotropic material to an incident P-wave[3] was utilized by Phinney[4] to define the crustal transfer function ratio

$$T_p(\omega) = W_o(\omega)/U_o(\omega) \quad .$$

$W_o(\omega)$ and $U_o(\omega)$ are the spectra of the vertical and horizontal components of displacement at the free surface, respectively. $T_p(\omega)$ is independent of the spectrum of the incident P-wave and depends only on the angular frequency ω and the apparent velocity c. The position of the peaks and troughs in $T_p(\omega)$ is relatively insensitive to changes in phase velocity and sufficiently sensitive to changes in the crustal model parameters to be useful in discriminating between competing crustal models. Phinney proposed that appropriate models for the crust and upper mantle beneath a recording station could be selected by matching $T_p(\omega)$ for a suite of crustal models to experimental transfer function ratios computed from the Fourier analysis of observed displacements or velocities of P-waves from distant earthquakes.

Crustal and upper mantle structure beneath LASA appears to be complex – certainly not well-suited to analysis in terms of the plane-layered crustal models assumed in the Haskell-Thomson theory. Using station travel time residuals at LASA, Greenfield and Sheppard[5] proposed a two-dimensional crustal structure extended in the NE to SW direction. Their model featured a decrease in crustal thickness of 11 km with a lateral distance of 35 km (see Fig. III-11). Glover and Alexander[6] analysed a variety of data and concluded that the maximum lateral change in structure across LASA is in a NE to SW direction. Iyer, et al.,[7] find evidence for complex structure beneath the central region of LASA and propose a synclinal structure trending toward the NE with 5 km of crustal thickening within the D ring.

Phinney found that the character of the long-period spectral ratio is sensitive to the gross structure beneath the recording site.[4] The matched 3-component long-period seismometers located at each of the LASA subarray centers provide the opportunity to obtain experimental transfer function ratios over a limited portion (0.05 to 0.2 cps) of the long-period spectral band (see Figs. III-12 and III-13). The frequency of the first (lowest frequency) peak in the transfer function ratio is diagnostic of the vertical P-wave travel time through the crust.[8]

The transfer function ratio samples structure near the recording site on an azimuth toward the source epicenter. The lateral resolution is about a crustal thickness[8] (~50 km for the Montana LASA) so that crustal model parameters determined from transfer function ratios represent structure averaged over a lateral distance of about 50 km from the subarray center toward the source epicenter. Transfer function ratios for events from three azimuths have been computed following the analysis scheme outlined by Bakun.[8] Composite transfer function ratios (the mean at each frequency of the transfer function ratios for the events listed in Table III-1) for each subarray-azimuth pair are shown as solid traces in Fig. III-14. The composite ratio (mean) ± its standard deviation is shown in Fig. III-14 as a dashed line. The number of events used to define each composite ratio is given in parentheses. The lowest frequency peak in the composite transfer function ratio is scored by a vertical line. A question mark adjacent to the vertical line indicates that the data are of poor quality. Composite transfer function ratio data were judged to be of poor quality if (a) only one event was available for the subarray-azimuth pair, (b) the

TABLE III-1

EVENTS STUDIED

Number	Date	Origin Time* (GMT)	Epicentral Coordinates*	Focal Depth (km)	Magnitude	Azimuth from center of subarray A0 (deg)	Distance from center of subarray A0 (deg)	Angle of Incidence† (deg)
1	15 February 67	16:11:11.8	9.0°S, 71.3°W (Peru-Brazil Border)	597	6.2	140.8	63.6	27.1
2	27 December 67	09:17:55.7	21.2°S, 68.3°W (Chile-Bolivia Border)	135	6.4	143.7	75.8	23.9
3	19 June 68	08:13:35.0	5.6°S, 77.2°W (No. Peru)	28	6.4	145.3	58.1	30.3
4	28 September 68	13:53:35.3	13.2°S, 76.4°W (Coast of Peru)	70	6.0	147.8	65.3	27.5
5	11 March 68	08:26:32.8	16.2°S, 173.9°W (Tonga Is.)	112	6.0	242.9	87.1	20.3
6	19 January 67	12:40:12.6	14.8°S, 178.8°W (Fiji Is.)	18	6.6	247.4	89.1	19.9
7	12 June 68	13:41:50.7	39.5°N, 142.7°E (Honshu Is., Japan)	44	6.0	311.5	74.5	24.5
8	3 August 68	04:54:32.7	25.6°N, 128.5°E (Ryukyu Is.)	19	6.4	312.4	92.7	19.3
9	14 May 68	14:05:06.0	29.9°N, 129.4°E (Ryukyu Is.)	168	5.9	314.2	88.7	19.9
10	5 August 68	16:17:04.8	33.3°N, 132.3° (Shikoku Is., Japan)	41	6.3	314.2	84.6	21.1

* Hypocenter parameters from USCGS PDE cards.

† Angle of incidence at the base of the crust computed from the Jeffreys-Bullen travel time tables with P_n = 8.0 km/sec.

standard deviation of the composite ratio was large, (c) the resolution of the lowest frequency peak was poor, or (d) agreement in the position of the first peak in the ratios for individual events with the composite ratio was poor.

The periods of the lowest frequency peaks, marked by a vertical line in Fig. III-14, are plotted on a map of the Montana LASA in Fig. III-15. Data marked by a question mark in Fig. III-14 are not shown in Figure III-15. Contours of the periods indicate the shape of structure beneath the Montana LASA. A shorter-period transfer function ratio first peak implies a smaller vertical P-wave crustal travel time and also a smaller crustal thickness, assuming a constant average crustal velocity.

The structure beneath LASA shown in Fig. III-15 is characterized by two trends: (1) crustal thinning from the northeast to the southwest across the array; and (2) a synclinal structure in the southwest quadrant of the array with axis trending to the northeast. Thus the structure proposed in Fig. III-15 is in agreement with the important features of the previously cited studies of structure beneath LASA.

The Haskell-Thomson theory assumes crustal models of plane-parallel layers of homogeneous isotropic material. It is interesting to note that a consistent picture of the complicated structure beneath LASA can be obtained using this theory. Nineteen of the fifty-one composite ratios shown in Fig. III-14 were judged reliable enough to use in constructing the crustal structure contours in Fig. III-15. Since the lateral resolution of the transfer function ratio is a crustal thickness, more rapid lateral variations in structure can be expected to result in data of poor quality. Scatter in the periods plotted in Fig. III-15 between the D and E rings near the E4 subarray is an indication of rapid lateral variation in crustal structure. It is interesting to note that the area lies atop Porcupine Dome, the most significant structural feature shown on geologic maps of the LASA region.

W. H. Bakun
(M.I.T., Dept. of Earth
and Planetary Sciences)

E. SPURIOUS LONG-PERIOD RECORDINGS AT LASA

A difficulty has been identified concerning the response of the long-period recording system at LASA. The nature of the problem is shown in Fig. III-16. The upper seismic traces in Fig. III-16 represent the vertical motion of the Rayleigh wave from a large Nevada Test Site (NTS) explosion recorded by the long-period instrumentation at sites C3 and D2. As seen in the figure, the two signals are quite similar up to about 140 sec from the beginning of the trace. Following 140 sec, however, the C3 trace shows a large, long-period arrival which does not appear on the trace of site D2. The spectral effects of this long-period motion are shown in Fig. III-16 where the spectral moduli of the time traces are plotted. The fine lines in the spectral diagrams are computed from the upper time series data. They show, due to the long period motion at C3, that the spectrum peaks at about 0.02 cps; whereas, that due to D2 exhibits a maximum at about 0.04 cps, although there is a small indication of a longer period ingredient to the wave train. On the lower time series traces in Fig. III-16 we have applied an artificial window to include only the fundamental Rayleigh wave motion and to exclude the late-arriving, ultra-long period motion at C3. The spectra computed from the windowed data are represented by the heavy line in the spectral diagram and are seen to be quite similar.

Because the ultra-long-period motion seen on trace C3 does not appear to propagate with regular amplitude across the array and because it does not exhibit a group velocity identifiable with any recognized seismic phase of these periods, at present we take this motion to be a spurious effect of the recording system.

It has been independently observed[9] that spurious long-period oscillations can occur in the output amplifier stage of the long-period system, the period of this oscillation ranging between 50 and 100 sec. This spurious signal is produced whenever a high-frequency (2.0 to 5.0 sec) signal is applied to the input terminals of the output amplifier stage. It is believed that an electrolytic capacitor (designed to shape the high frequency response) in the output amplifier stage produces the long-period oscillation in response to high-frequency signal inputs. This spurious response is also termed inter-modulation distortion. Since this capacitor is relatively large in physical size, as well as in capacitative value, it has been kept at the output stage of the system, otherwise extraneous signals would be introduced due to electrical coupling. It may be possible to eliminate this problem by placing it, with some care, at some stage preceding the output amplifier stage.

In practice, the high-frequency component may be introduced by the seismic phases Lg or Rg observed at regional distances over continental paths. It is important to note that these phases are not commonly observed for $\Delta > 40°$ so that any spurious long-period signal they introduce should not be a problem in the teleseismic distance range.

If these high-frequency seismic phases induce spurious long-period components in the sensors at LASA, they should have an apparent phase velocity which is about the same as the group velocity of the high-frequency signals. This test has been performed and it has been found that the direction and phase velocity of the spurious long-period signal correspond to the direction and group velocity measured for the Rg phase. The measurement of the phase velocity of the long-period signal was done using the high-resolution wavenumber analysis program applied to the array of long-period vertical sensors at LASA. The group velocity measurements for the Rg phase were made by using the high-resolution wavenumber analysis program applied to subarrays of short-period vertical sensors at LASA. Thus, there is strong evidence to indicate that for events in the non-teleseismic range, which have large Lg or Rg phases, there will be a spurious long-period component introduced at LASA. This is unfortunate, and measures should be taken to remove this limitation. This is especially relevant in view of the importance of close-in observations of the Rayleigh wave in order to improve signal-to-noise ratios for the application of the M_s-m_b discriminant.

It should also be noted that the anomalous wavenumber measurements obtained by Mack at 0.015 cps, or 67 sec period, and reported in SATS (31 December 1969, DDC AD-700322) for events from the NTS, were quite likely due to the spurious long-period signals described previously.

J. R. Filson
J. Capon

REFERENCES

1. D. Davies, E.J. Kelly and J.R. Filson, "The Vespa Process for the Analysis of Seismic Signals," Nature 232, 8-13 (1971).
2. J. Capon and N.R. Goodman, "Probability Distributions for Estimators of the Frequency-Wavenumber Spectrum," Proc. IEEE 58, 1785-1786 (October 1970).
3. N.A. Haskell, "Crustal Reflection of Plane P and SV Waves," Bull. Seismol. Soc. Am. 43, 17-34 (1962).
4. R.A. Phinney, "Structure of the Earth's Crust from Spectral Behavior of Long-Period Body Waves," J. Geophys. Res. 69, 2997-3017 (1964).
5. R.J. Greenfield and R.M. Sheppard, "The Moho Depth Variations under the LASA and Their Effect on $dT/d\Delta$ Measurements," Bull. Seismol. Soc. Am. 59, 409-420 (1969).
6. P. Glover and S.S. Alexander, "Lateral Variations in Crustal Structure Beneath the Montana LASA," J. Geophys. Res. 74, 505-531 (1969).
7. H.M. Iyer, A.R. Jackson, J.H. Healy and T.E. Landers, "LASA Anomalies and Their Relations to Crust and Upper Mantle Structure," U.S. Geol. Survey Open File Report (1970).
8. W.H. Bakun, "Crustal Model Parameters from P-Wave Spectra," Bull. Seismol. Soc. Am. (in press).
9. M. Gudzin, Geotech, personal communication.

Section III

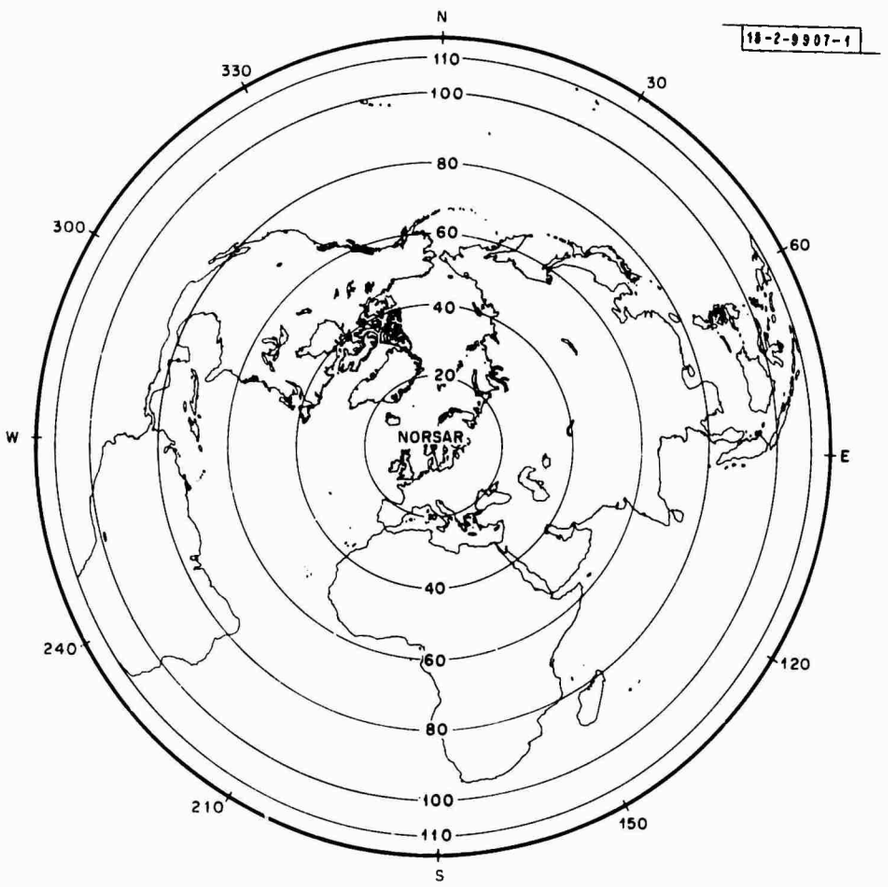

Fig. III-1. World equidistont-ozimuthol projection centered on NORSAR.

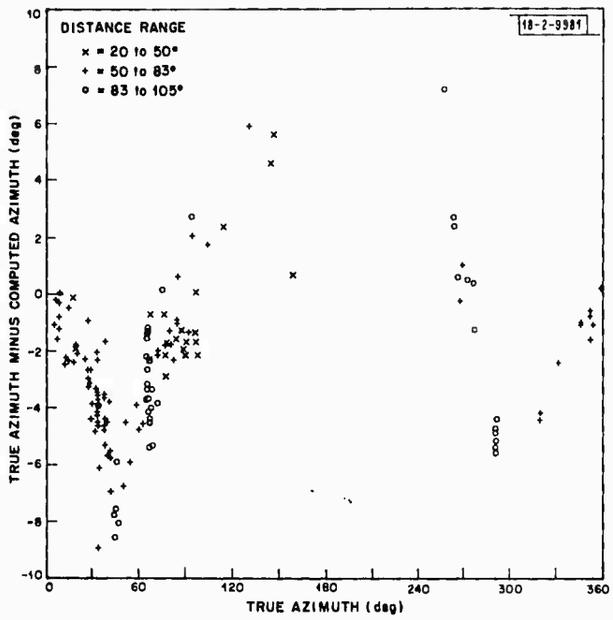

Fig. III-2. NORSAR azimuth errors.

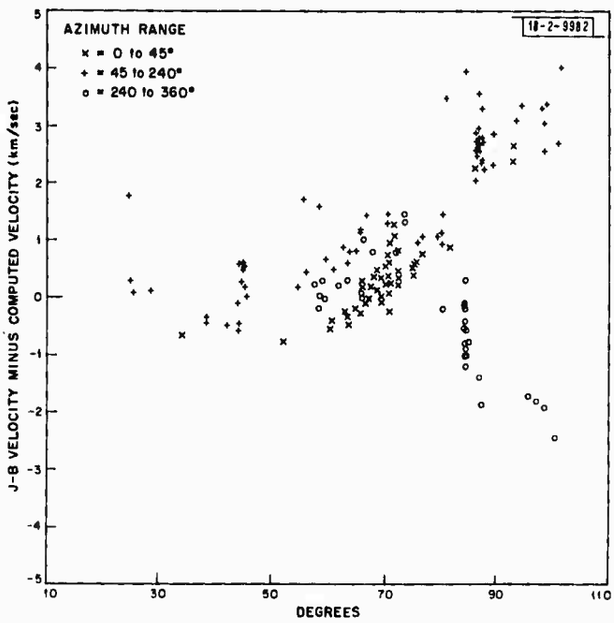

Fig. III-3. NORSAR errors in horizontal phase velocity.

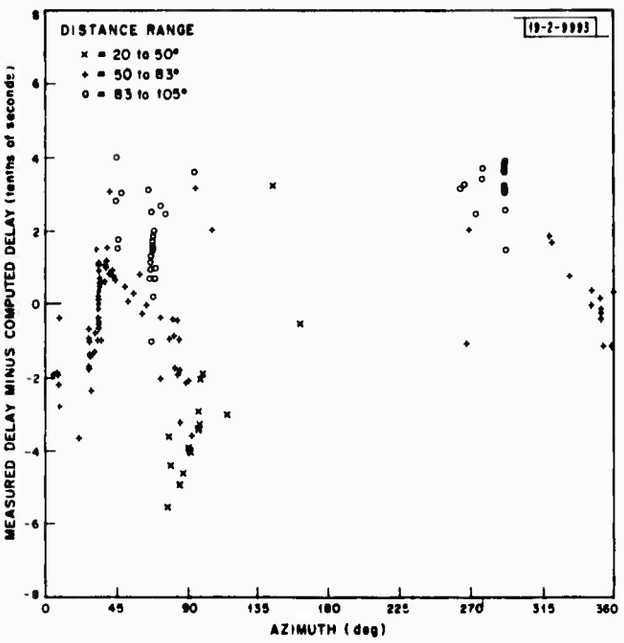

Fig. III-4. Site 7B J-B travel time errors relative to 4C (azimuth).

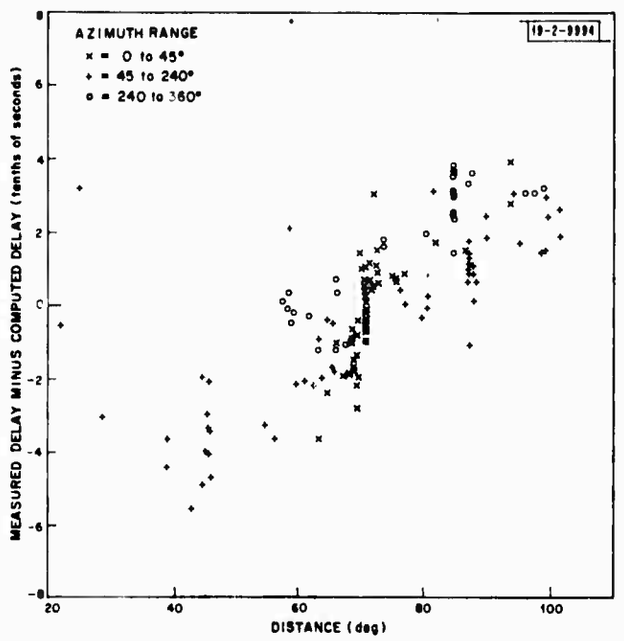

Fig. III-5. Site 7B J-B travel time errors relative to 4C (distance).

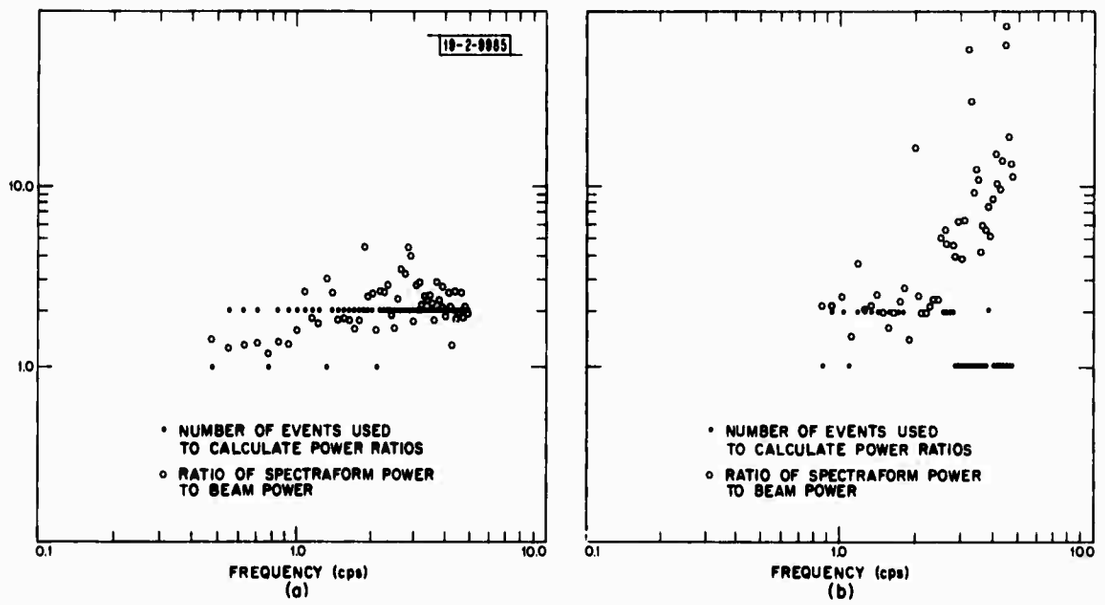

Fig. III-6. Spectraform improvement over beomform in spectral determinations: (a) events ~20° from NORSAR; (b) events ~40° from NORSAR.

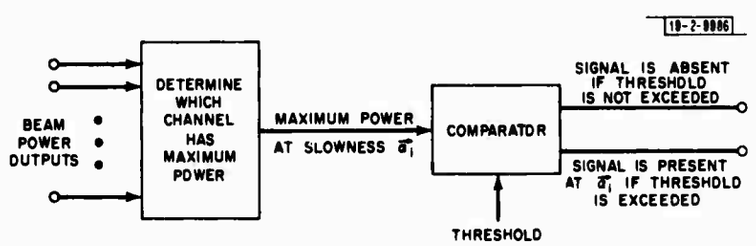

Fig. III-7. Block diagram for the implementation of the optimum decision rule for interpretation of either Vespagram or Beamsplit data.

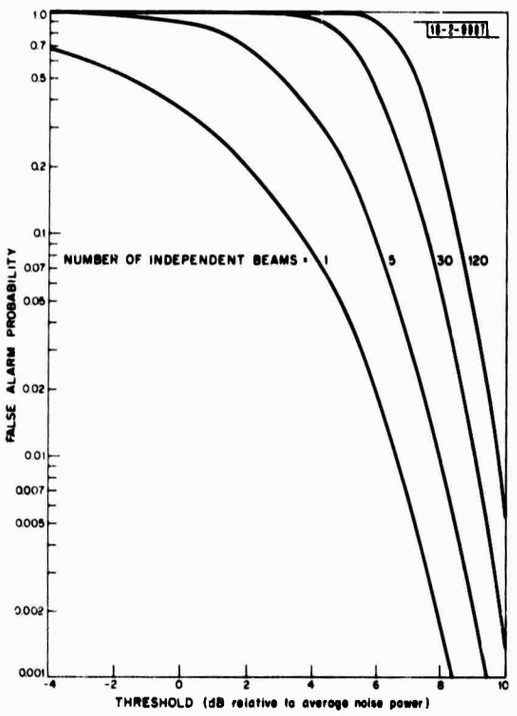

Fig. III-8. False alarm probability vs threshold for various numbers of independent beams.

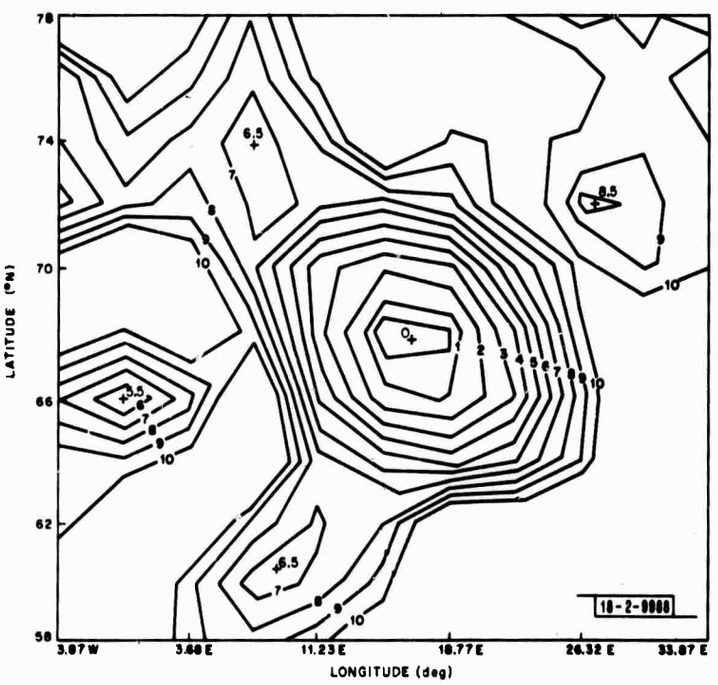

Fig. III-9. Beamsplit data for the South West Russia event. Contours are at 1 dB intervals. The display is centered on 68°N, 15°E and has an aperture of about 2000 km.

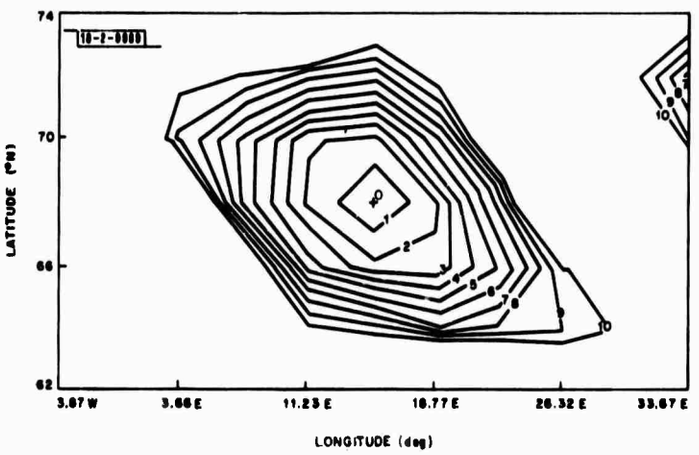

Fig. III-10. The theoretical beam pattern for signal emerging from 68°N, 15°E. The display has the same parameters as those of Fig. III-9.

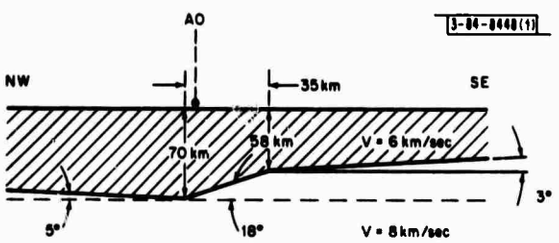

Fig. III-11. Cross section of the crustal model for LASA from Greenfield and Sheppard.[5]

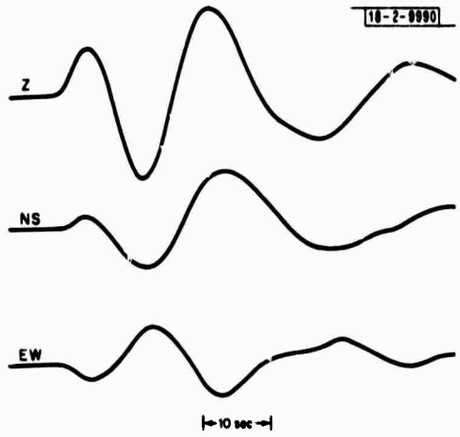

Fig. III-12. Vertical (Z), north-south (NS) and east-west (EW) components of the 15 February 67 South America event (see Table III-1) recorded on the long-period seismometers of the center of subarray F3.

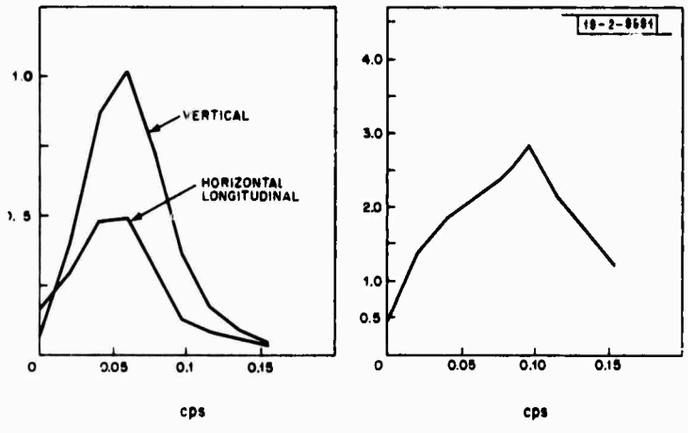

Fig. III-13. Moduli (left) of the Fourier transforms of the vertical and resolved horizontal longitudinal components for the event shown in Fig. III-12. The transform moduli are normalized to the maximum of the vertical spectrum. The transfer function ratio (right) is the vertical spectrum divided by the resolved horizontal longitudinal spectrum.

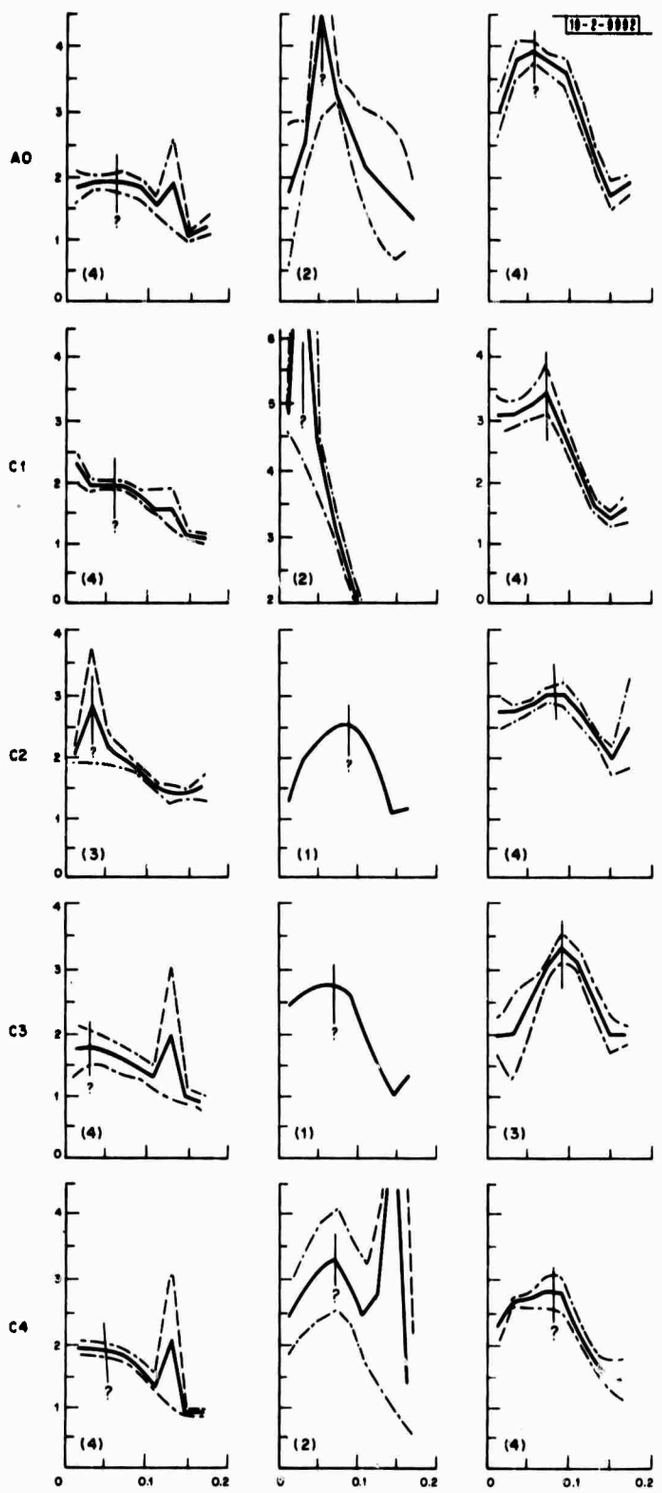

Fig. III-14(a). Composite transfer function ratios (solid traces) for the subarrays A0, C1, C2, C3 and C4 for the South America events (left column), the Fiji-Tonga events (middle column) and the Japan events (right column) as a function of frequency (cps).

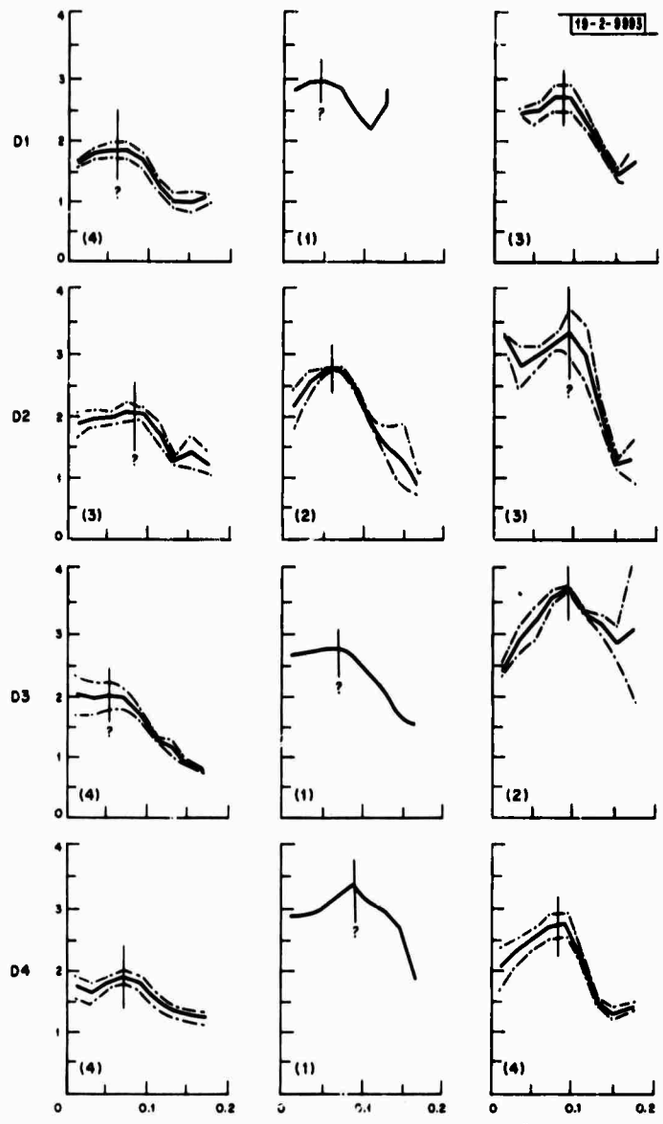

Fig. III-14(b). Composite transfer function ratios for the D1, D2, D3 and D4 subarrays. See legend for Fig. III-14(a).

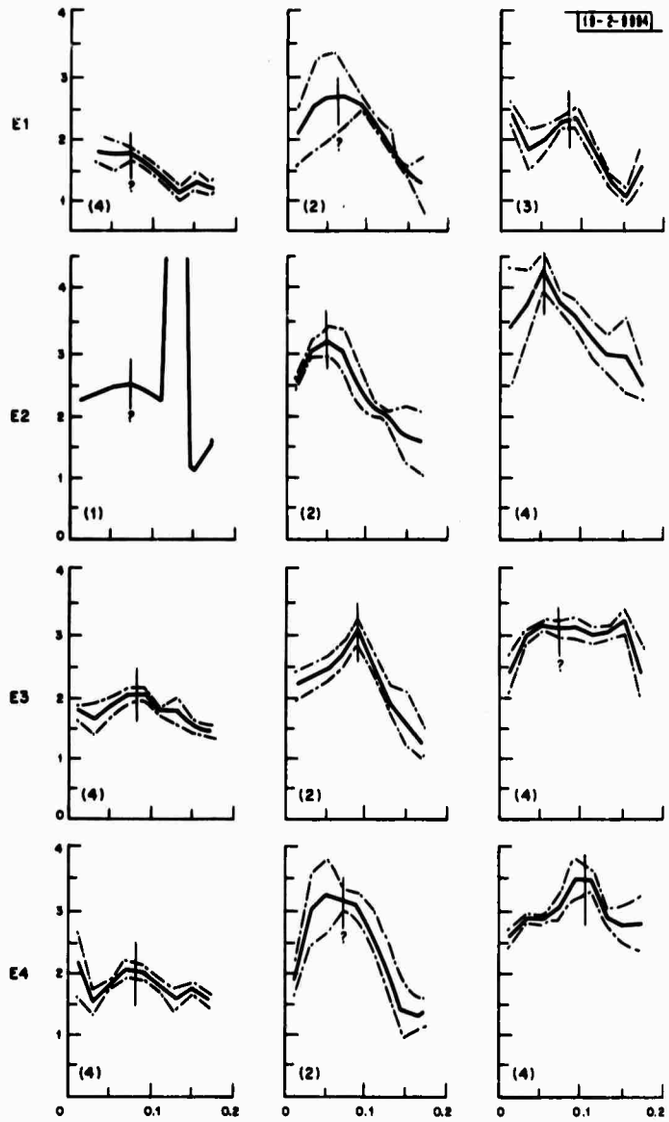

Fig. III-14(c). Composite transfer functian ratias far the E1, E2, E3 and E4 subarrays. See legend for Fig. III-14(a).

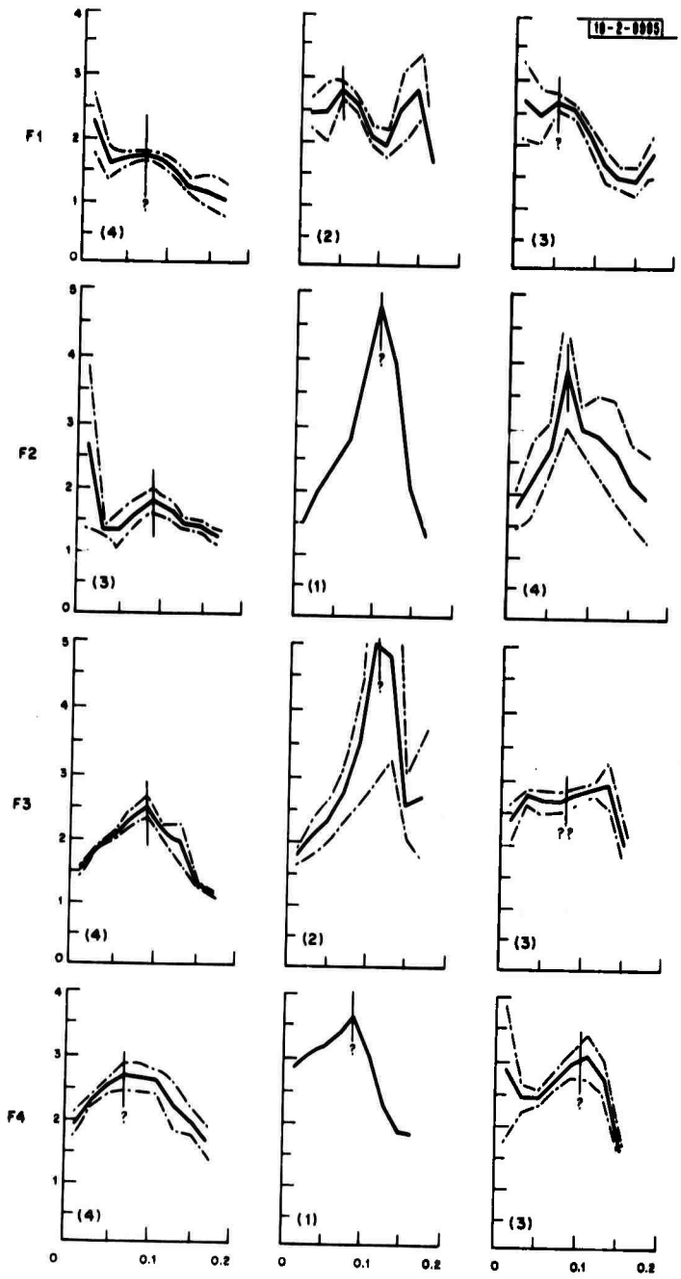

Fig. III-14(d). Composite transfer function ratios far the F1, F2, F3 and F4 subarrays. See legend for Fig. III-14(a).

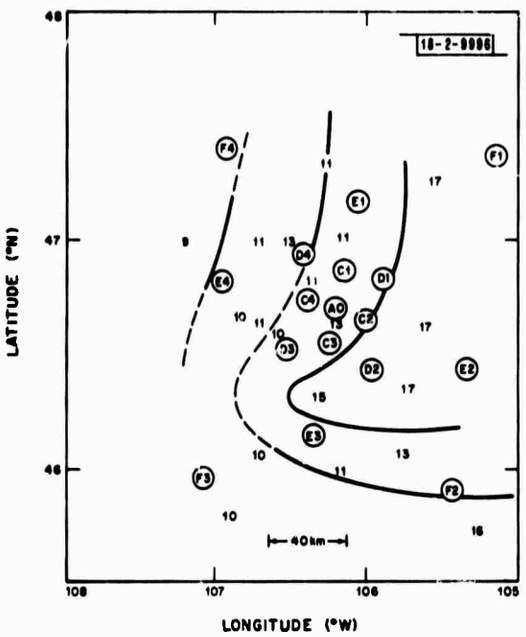

Fig. III-15. Map of LASA. The periods of the lowest frequency peaks of the composite transfer function ratios (Fig. III-14) are plotted 25 km, ~ 1/2 the crustal thickness beneath LASA, from the subarray centers along the azimuth toward the appropriate source epicenter.

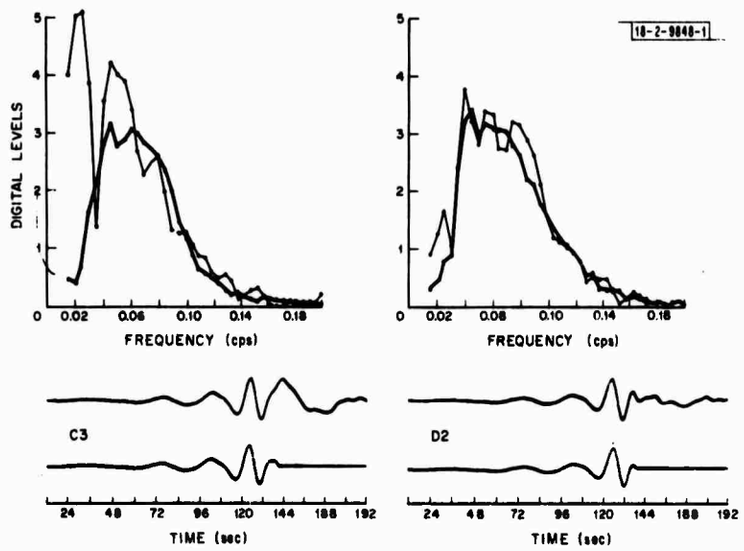

Fig. III-16. Spectral effects (fine line) of late arriving long period motion which is present at C3, but absent at D2. The narrower window of the lower seismic traces renders the spectra (heavy line) of this vertical motion due to the Rayleigh wave practically identical at the two sites.

IV. LINCOLN-BASED DATA PROCESSING FACILITIES

A high speed, high quality, hard-copy electrostatic output device (GOULD 4800) has been added to our PDP-7's. This plotter can be switched to either computer as required. As an auxiliary line printer it is very fast and silent – 4800 lines per minute. As a general graphical output, it features a resolution and accuracy of 1/80 inch. The size of the output graphics is 10 inches (800 points) in one dimension and unlimited in the other dimension.

The software has been modified so that all pictures from the Data Analysis Console and all DISPAC produced pictures can be output on the GOULD. The PLOT program has been generalized and rewritten to plot data in any of our standard tape formats directly on space to the GOULD or the SANBORN plotters.

P. L. Fleck